Dual-Band Dual-Linear-to-Circular Polarization Converter in Transmission Mode Application to *K*/*Ka*-Band Satellite Communications

Parinaz Naseri, *Member, IEEE*, Sérgio A. Matos, *Member, IEEE*, Jorge R. Costa, *Senior Member, IEEE*, Carlos A. Fernandes, *Senior Member, IEEE*, and Nelson J. G. Fonseca, *Senior Member, IEEE*

***Abstract*— Many wireless communication applications such as satellite communications use circularly polarized (CP) signals, with the requirement for easy switching of the polarization sense between uplink and downlink. Specifically, in satellite communications, the trend is also to move to higher frequencies and integrate the receiving and transmitting antennas in one dual-band terminal. However, these simultaneous demands make the design and fabrication of the composing parts very challenging. We propose, here, a dual-band dual-linear polarization (LP)-to-CP converter that works in the transmission mode. The working principle of this polarizer is explained through an example for Ka-band satellite communications at 19.7–20.2 and 29.5–30 GHz. The LP-to-CP converter is a single panel composed of identical unit cells with a thickness of only 1.05 mm and a size of 5.3 mm × 5.3 mm. Due to its operation in the transmission mode, the polarizer can be combined with a simple dual-band dual-LP antenna to obtain the desired dual-band dual-CP single antenna. However, the unique property of this polarizer is yet the fact that it converts a given LP wave, e.g., x-polarization, to orthogonal CP waves at the two nonadjacent frequency bands, e.g., left-handed CP at lower band and right-handed CP at higher band. The polarizer is tested both with 20 and 30 GHz LP rectangular horns to illuminate a dual-band transmit array (TA) to obtain wide-angle steering of CP beams. The performance of the polarizer and its association with the TA is evaluated through simulation and measurements. We also present design guidelines for this type of polarizer.**

***Index Terms*— Antenna–filter–antenna, circular polarization (CP), dual-band antennas, frequency selective surfaces, periodic structures, polarization conversion.**

The func
is confirr
is require

AQ:1

Manuscri[illegible]d May 3, 2018; revised July 21, 2018; accepted October 4, [illegible]s work was supported in part by the European Space Agency under Contract 4000109111/13/NL/AD and in part by the Fundação para a Ciência e Tecnologia under Project PEstOE/EEI/LA/0008/2013 and Project UID/EEA/50008/2013. *(Corresponding author: Parinaz Naseri.)*

AQ:2

~~P. Naseri and~~ C. A. Fernandes are with the Instituto de Telecomunicações, 1049-001 Lisbon, Portugal, and also with the Instituto Supe-rio[illegible]ersidade de Lisboa, 1049-001 Lisbon, Portugal (e-mail: pa[illegible].pt).

Confirmed. N
is required.

AQ:3

S. A. Matos and J. R. Costa are with the Instituto de Telecomunicações, 1049-001 Lisbon, Portugal, with the Instituto Superior Técnico, Universidade de Lisboa, 1049-001 Lisbon, Portugal, and also with the Departamento de Ciências e Tecnologias da Informação, Instituto Universitário de Lisbon, 1649-026 Lisbon, Portugal.

N. J. G. Fonseca is with the Antenna and Sub-Millimetre Wave Section, European Space Agency, 2200 AG Noordwijk, The Netherlands (e-mail: nelson.fonseca@esa.int).

Color versions of one or more of the figures in this paper are available online at http://ieeexplore.ieee.org.

Digital Object Identifier 10.1109/TAP.2018.2874680

I. Introduction

In SOME applications such as satellite and point-to-multipoint communications, circular polarization (CP) is preferred over linearly polarized (LP) radiation because it is less influenced by multipath fading and by polarization mismatch associated with ground terminal mobility [1].

For satellite communications (satcom), besides CP, an antenna is usually required to operate at two distinct and nonadjacent frequency bands in orthogonal polarizations as a means to further enhance the isolation between transmit and receive signals, as power flux densities for those types of applications are very low and particularly sensitive to interference. For example, broadband satellite communications at *Ka*-band make use of a dedicated frequency spectrum with the downlink (D/L) at 19.7–20.2 GHz and the uplink (U/L) at 29.5–30 GHz. If the user (ground) terminal receives (D/L) a left-handed CP (LHCP) electromagnetic (EM) field, it should transmit (U/L) an orthogonal EM field, in this case, a right-handed CP (RHCP) field. Another important aspect for mobile satcom applications associated with spot beam broadband satellites is the polarization diversity over the service area, meaning that the user terminal must be able to switch from one polarization to another in both bands, while maintaining the polarization orthogonality between the two bands when doing the handover between one spot and the adjacent one.

In order to respond to these requirements, user terminal antennas for *Ka*-band satcom often use a horn antenna combined with an orthomode transducer to feed a reflector [2], [3] or transmit array (TA) [4], [5]. Alternatively, the terminal antenna may be a phased array of dual-band dual-CP patch antennas [6]–[9]. However, these solutions are either bulky and expensive or compact but inefficient and hard to fabricate at *Ka*-band frequencies. There is a demand for simpler solutions, low profile, low cost, and easy to fabricate up to millimeter-wave frequencies. In general, CP waves can be generated by antennas such as the truncated microstrip patch, crossed dipoles [6], helix, and spiral [1]. However, none of these allows dual band, unidirectional radiation patterns with moderate directivity (e.g., 10–20 dBi) in a simple implementation without the need for a polarization device, typically a hybrid directional coupler.

The literature offers another way of generating CP EM fields by combining an LP antenna and a polarization converter to avoid the above-mentioned shortcomings of conventional CP antennas. The polarization converter is basically an anisotropic medium that fully transmits (or reflects) a given LP field with a 90° phase difference along its two main axes, orthogonal to the direction of propagation. Hence, an incoming slant LP field, i.e., at 45° with respect to the two main axes, will be converted into a CP field. This sort of medium has been generally implemented using existing materials and various different metallic element designs in planar periodic structures such as frequency selective surfaces [11]–[16] and metasurfaces [17]–[19]. The existing LPs-to-CPs are mostly either wideband [11]–[13] or single band [14]–[18]. In [19], a very interesting polarizer based on a chiral cell geometry is used to convert an incident LP wave into orthogonal handedness CP waves in a low band and a high band. However, it only works for x-LP incident wave, imposing a fixed CP handedness at the low and high bands. This precludes the use of this type of cell for mobile satellite applications requiring polarization switching for handover purposes as described earlier. In [20], a polarization converter in the reflection mode was introduced, having a dual-band dual-polarization capability with the desired polarization orthogonality between the two separate operating bands from the same incident LP field. This characteristic, considered for the space segment in [20]–[22], is demonstrated here with a polarization converter in transmission mode for the ground segment, and more specifically user terminals. Using a TA instead of a polarizing reflector design allows for reduced antenna height, which is desirable for mobile user terminal applications. In addition, the dual-band dual-polarization characteristic would enable the design of a TA antenna with a simplified feed design, either a single-polarized feed, eventually rotating 90° for handover purposes, or a dual-polarized feed combined with a single-wideband switch, also for handover purposes.

This paper focuses on a new compact and efficient dual-band dual-CP that can be used to create an antenna satisfying all the previously identified aperture-feeding requirements for user terminals in multispot satellite communication systems. In fact, we propose a novel and low-loss dual-band dual-LP-to-CP converter to be operated in combination with a simple dual-band dual-LP feed antenna. We demonstrate the performance of the polarizer fed by an LP horn to illuminate a high-gain dual-band wide-angle beam steering TA. Together they form a low-profile dual-band dual-CP user terminal antenna for *Ka*-band satellite communications. We further present design rules for the polarizer.

This paper is organized as follows. In Section II, different components of the overall proposed antenna are presented and described. In Section III, the unit cell (UC) of the LP-to-CP converter is introduced and the effects of different physical parameters on the frequency response of the UC are explained. Section IV presents the simulation and measurement results of two horns at 20 and 30 GHz combined with the polarization converter. Finally, in Section V, the combinations of the horns and the polarizer are employed to feed a dual-band TA to implement a low-profile dual-band dual-CP ground terminal for *Ka*-band satellite communication.

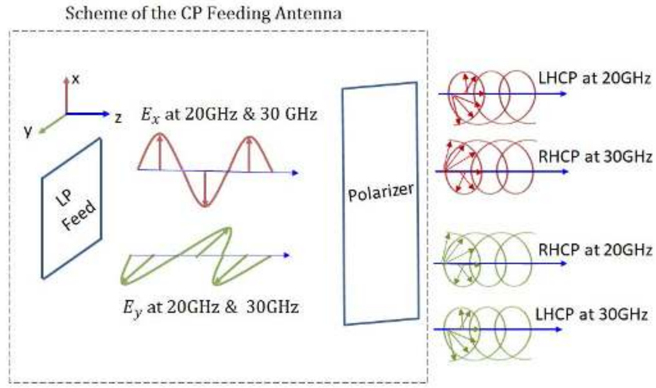

Fig. 1. Scheme of the dual-band dual-CP antenna to feed a large aperture for *Ka*-band satellite communications. It is composed of the dual-band LP feed and a dual-band LP-to-CP.

II. Antenna Configuration

Fig. 1 shows the scheme of the proposed dual-band dual-CP antenna to feed a large aperture for *Ka*-band satellite communications. The feed element excites two orthogonal LPs at two frequency bands. Each LP illuminates the polarizer and gets converted to two orthogonal CPs at the two frequency bands. Note that, for the same input LP, the output CP is orthogonal between the U/L and D/L bands. The design of a dual-band linear antenna to feed the polarizer is out of the goals of this paper. Therefore, in this paper and as a proof-of-concept, the LP waves at 20 and 30 GHz are radiated by two LP rectangular horns operating at these respective frequencies.

The proposed LP-to-CP converter is a single panel composed of identical UCs. These elements have dual-band operation with the low insertion loss at both bands. Besides, the polarizer is physically and electrically very thin (only 1.05 mm, corresponding to $0.07\lambda_0$ and $0.11\lambda_0$ at 20 and 30 GHz, respectively).

The working principle of the polarizer starts with the splitting of an LP wave into two orthogonal linear components, like standard polarization converters do. However, it then generates −90° phase shift between them at the lower frequency band and +90° phase shift at the higher frequency band. This means that a linear x-polarized incident wave at the lower frequency band gets converted to an LHCP wave through the polarizer, while the same LP wave gets converted to an RHCP wave at the higher frequency band. The polarizer functions the same way for a linear y-polarized incident wave, but it converts into the orthogonal CP wave at each band compared to the x-polarized incidence.

III. Linear-to-Circular Polarizer Unit Cell

The UCs that compose the proposed LP-to-CP converter present x'- and y'-axes symmetries [$x'y'z'$ is the local coordinate system of the cell, rotated 45° around the z-axis with respect to the main xyz coordinate system, see Fig. 2(a)], and are similar to the ones introduced in [25]–[28].

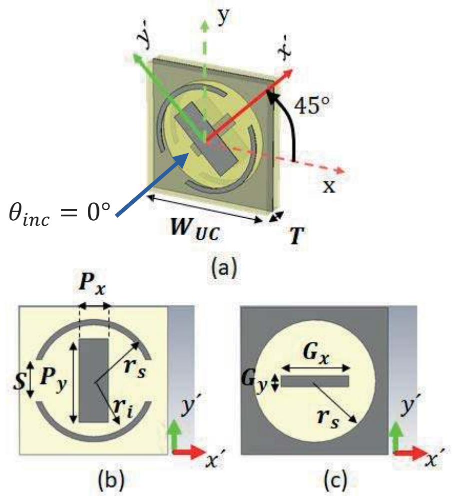

Fig. 2. Structure of the UC. (a) 3-D view. (b) First layer. (c) Second layer.

Once an LP incident wave makes a ±45° angle in relation to the x'- and y'-axes of the cell [Fig. 2(a)], the cell decomposes the wave into two orthogonal components along x'- and y'-axes. To avoid generating a +45° directed incident wave, we rotated the cell by 45°. Then, it transmits both components with almost equal amplitude and −90° phase difference at 20 GHz and +90° phase difference at 30 GHz. For example, the +45°-rotated UC converts a y-polarized incident wave to an RHCP at 20 GHz and to an LHCP at 30 GHz through the polarizer.

The cell is composed of three metallic layers parallel to the $x'y'$ plane, separated by thin 0.508 mm dielectric Rogers DuroidTM 5880 slabs ($\varepsilon_r = 2.2$ and $tan\delta = 0.0009$). The first and the third layers of the UC are identical and composed of a patch and a split ring. The middle layer is composed of a circular slot plus a rectangular patch.

Due to the asymmetric elements along x'- and y'-axes (lack of 90° rotational symmetry), the UC responds differently to the two orthogonal LP and normal incident waves (i.e., x′-polarized and y′-polarized waves). To operate as an LP-to-CP converter, the cell should transmit both x'- and y'-polarized waves with equal amplitude and 90° phase difference. The proposed UC shown in Fig. 2 provides this distinct response to x'- and y'-polarized normal incidences at two frequency bands.

The design and optimization of this UC were performed in CST Microwave Studio [29] using periodic boundary conditions in x'- and y'-directions and open in z'-direction so that it operates at dual-satellite communication *Ka*-band, i.e., 19.7–20.2 and 29.5–30 GHz. The structure is illuminated by two normal plane waves propagating in the z'-direction with the electric fields in x'- and y'-directions. The optimization aimed to obtain linear reflection coefficients below −10 dB; therefore, it is a very good transmission, while the phase difference between the two linear transmission coefficients was required to be about ±90° at both frequency bands. The optimized dimensions of the cell are summarized in Table I. The reflection coefficients of the UC for these normal incident waves are presented in Fig. 3. The gray bars in Fig. 3 highlight the two frequency bands of the dual-*Ka*-band satellite communications. Fig. 4(a) and (b) shows the amplitude and phase of the transmission coefficients of the cell for these orthogonal incidences. Based on these much different coefficients of the cell, it can be concluded that the cell presents distinct features to the x'- and y'-polarized waves.

TABLE I
DIMENSIONS OF THE UC

parameter	length (mm)	parameter	length (mm)
G_x	2.35	r_s	2.2
G_y	0.5	S	1.5
P_x	0.9	T	1.05
P_y	2.9	w_{UC}	5.3
r_i	1.85		

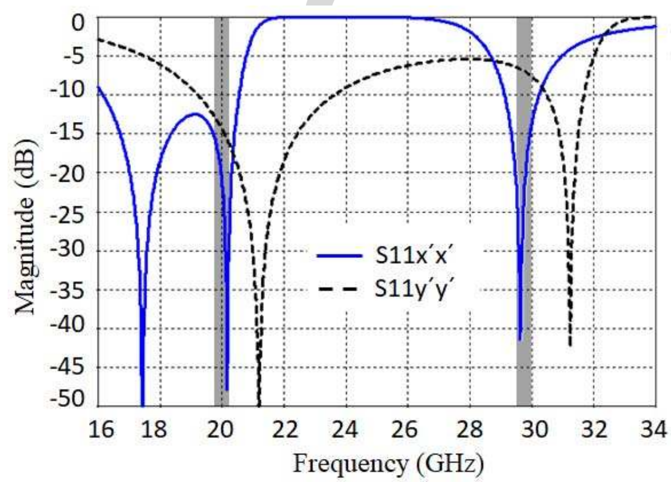

Fig. 3. Reflection coefficients of the UC for an x′-polarized and a y′-polarized normal incident waves.

A. Cell Design Guidelines

To design a similar cell for other frequencies, one should choose W_{UC} close to $\lambda/2$, where λ is the wavelength at the higher frequency band. It is also essential that the behavior of the reflection coefficients of the cell follows the one depicted in Fig. 3, where the first two resonances of the cell to an x′-polarized wave are below its resonance to an y′-polarized incident wave. Moreover, the third resonance to an x′-polarized wave is also less than the second resonance of the cell to y′-polarized wave. However, it is also important that the transmission coefficients of the cell follow the ones depicted in Fig. 4(a), where $S21x'x'$ has two zeros in the middle of the band. The two split rings behave as strongly coupled resonators for x′-polarized incident wave, while they are nonresonant for y′-polarized incident wave for frequencies below 30 GHz. This provides a 180° phase jump only in S21x′x′, between the two working bands, and consequently, enables opposite handedness in the transmitted CP waves in the two bands. The two identical rectangular patches in the same layers are used to achieve the transmission bands for the y′-polarized wave. Finally, the circular slot in the middle layer

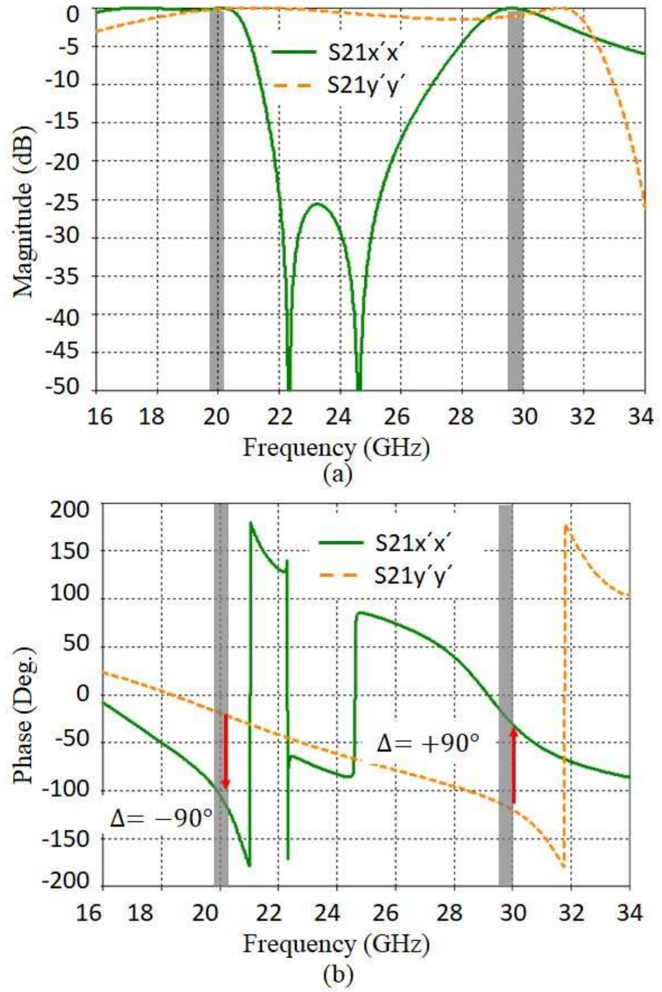

Fig. 4. (a) Amplitude and (b) phase of the transmission coefficients of the UC to an x′-polarized and a y′-polarized normal incident waves.

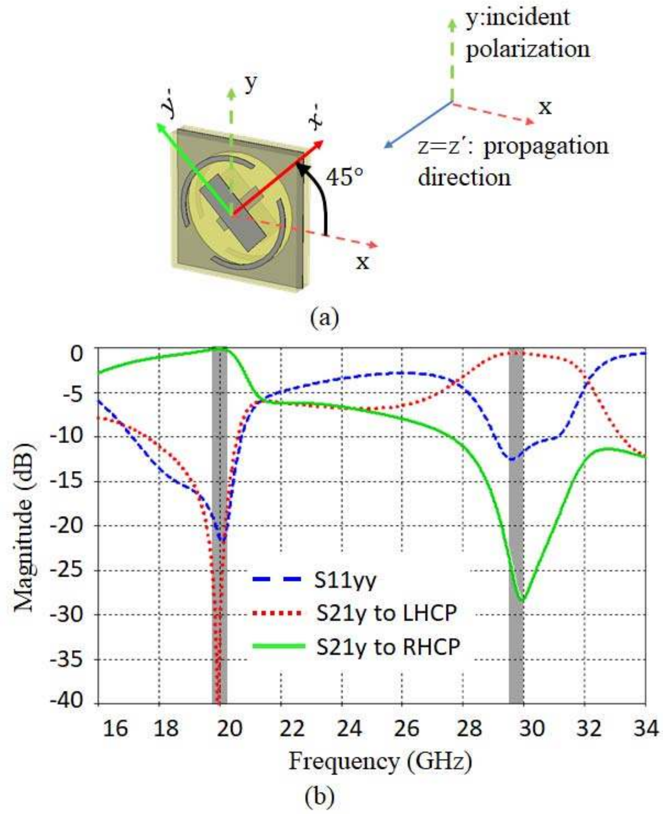

Fig. 5. Reflection coeffici~~ent and linear-to-circular transmission coefficients of the UC to y-polarized component normal incident wave and with the cell system of axis rotated by 45° in relation to the incident wave polarization.~~ AQ:5

provides the transmission bands in the lower band. Finally, Fig. 4(b) shows how this arrangement of the resonances allows achieving LP-to-CP conversion with orthogonal handedness at the two bands.

In order to achieve the mentioned resonances, one should choose r_s so that $c/(2\pi r_s\sqrt{\varepsilon_{\text{eff}}})$ is lower than the lower frequency band, where c is the speed of light in free space and ε_{eff} is approximated by $(\varepsilon_r + 1)/2$. This ensures that the first resonance in $S11$x′x′ is lower than the desired lower band edge, i.e., 19.7 GHz in the present example. It is worth mentioning that r_s is both the outer radius of the ring and the radius of the slot. This step helps finding the right substrate permittivity ε_r. In the subsequent step, the second resonance in the $S11$x′x′ has to be close to the lower desired frequency band and lower than the first resonance in $S11$y′y. This condition is necessary to obtain −90° phase difference between the two linear transmission coefficients at the lower frequency band (19.7–20.2 GHz). The second resonance in $S11$x′x is due to the strong coupling between the two split rings and can be achieved and altered by choosing a thinner substrate [30]. Therefore, a substrate thickness based on the available standard commercial size and meeting the previous step can be found. Additional tuning can be done by adjusting the width of the ring, $r_s - r_i$, to shift up this secondary resonance by increasing the width. The third resonance in $S11$x′x′ can be altered by the choice of G_x and G_y so that first, it would be close to the higher desired frequency band, 29.5–30 GHz, and second, it would be lower than the second resonance in $S11$y′y′ (Fig. 3).

For the y′-polarized incident wave, by choosing S, the size of the split in the rings, about $2r_s/3$ and P_y of about $4r_s/3$, the main behavior of the cell to the y′-polarized incident wave is almost defined. One can fine tune S11y′y′ by altering P_x to obtain ±90° phase difference in the transmission coefficient at both frequency bands and ensure that the second resonance of S11y′y′ is slightly higher than the third resonance of the $S11$x′x′. Of course, these guidelines define only the general behavior of the cell and its resonances. After these steps, fine tuning the dimensions through the full-wave simulation of the UC is required to obtain the final results.

B. Linear-to-Circular Polarization Conversion

To assess the insertion loss and the axial ratio of the CP transmitted fields by the polarizer UC, the response of the cell to a y-polarized field [Fig. 5(a)] is presented. The linear reflection and linear-to-circular transmissions of the cell to a y-polarized incident wave are shown in Fig. 5(b).

These coefficients are the same for an x-polarized incident wave but the cell converts the x-polarized of incident wave to an LHCP wave at 20 GHz and to an RHCP wave at 30 GHz with the same coefficients.

Based on Fig. 5(b), the insertion loss of the polarizer cell is 0.1 dB at 20 GHz and 0.6 dB at 30 GHz. This loss is higher at 30 GHz than 20 GHz due to higher reflections of the cell to both LP incident waves (Fig. 3). The bandwidths of the cell, where the reflection coefficient is less than −10 dB and the cross polarization is better than −15 dB, are about 4% (800 MHz) and 8% (2.3 GHz) at 20 and 30 GHz, respectively. The provided bandwidths are much wider than the bandwidths required for *Ka*-band satellite communication highlighted with gray shading in Fig. 5.

It is also important to assess the sensitivity of the cell's performance to the incidence angle. Fig. 6 presents the frequency response of the cell for incident angles up to $\theta_{inc} = 45°$. It is shown that for up to 45° oblique incidence, the transmission loss of the cell increases to only 0.65 dB within 19.7–20.2 GHz [Fig. 6(a)] and 3.2 dB in 29.5–30 GHz [Fig. 6(b)]. Moreover, the dependence of the axial ratio on the incident angle at the lower frequency band and the higher frequency band is presented in Fig. 6(c) and (d), respectively. Fig. 6 shows that the higher increase of transmission loss in the upper band is due to an increase in the reflection coefficient and not by a particular higher depolarization effect of the UC when compared to the lower band. The axial ratio is below 3 and 3.4 dB for incidence angles up to 45° at the lower and higher frequency bands, respectively. However, for incidence angles up to $\theta_{inc} = 30°$, the insertion loss is below 0.2 dB at the lower band and it is below 1.5 dB at the higher band. Moreover, for incidence angles up to $\theta_{inc} = 30°$, the axial ratio is better than 2.3 dB at both bands. While these results are only presented for y-polarized wave, they are also valid for an x-polarized wave but with orthogonal CPs at each band.

IV. Experimental Validation of the Polarizer

An 8 × 8 array of the LP-to-CP converter UC, introduced in Section III, was fabricated. Each layer was printed on 20 mil Rogers 5880 with 17μm cladding. Then, the printed layers were aligned and glued together with Rogers 3001 bonding film, which has the same relative permittivity as the Rogers 5880 substrate.

To evaluate the performance of the polarizer at both bands, it was first placed in front of a standard gain *K*-band rectangular horn (Flann Microwave N° 20240-15) with 14.4 dBi gain at 20 GHz. Then, it was placed in front of a *Ka*-band standard gain rectangular horn (Flann Microwave N° 22240-15) with the same gain of 14.1 dBi at 30 GHz. Fig. 7 shows the 3-D printed setup to hold the center of the polarizer in front of the center of the horn's aperture and parallel to it. As shown in Fig. 7, the radiation from the horn is y-polarized compared to the polarizer axis. The setup was designed to allow changing the distance between the polarizer and horn to optimize the axial ratio at both bands.

The distance between the polarizer and the horns was first set to $d = 22.5$ mm according to the simulation results.

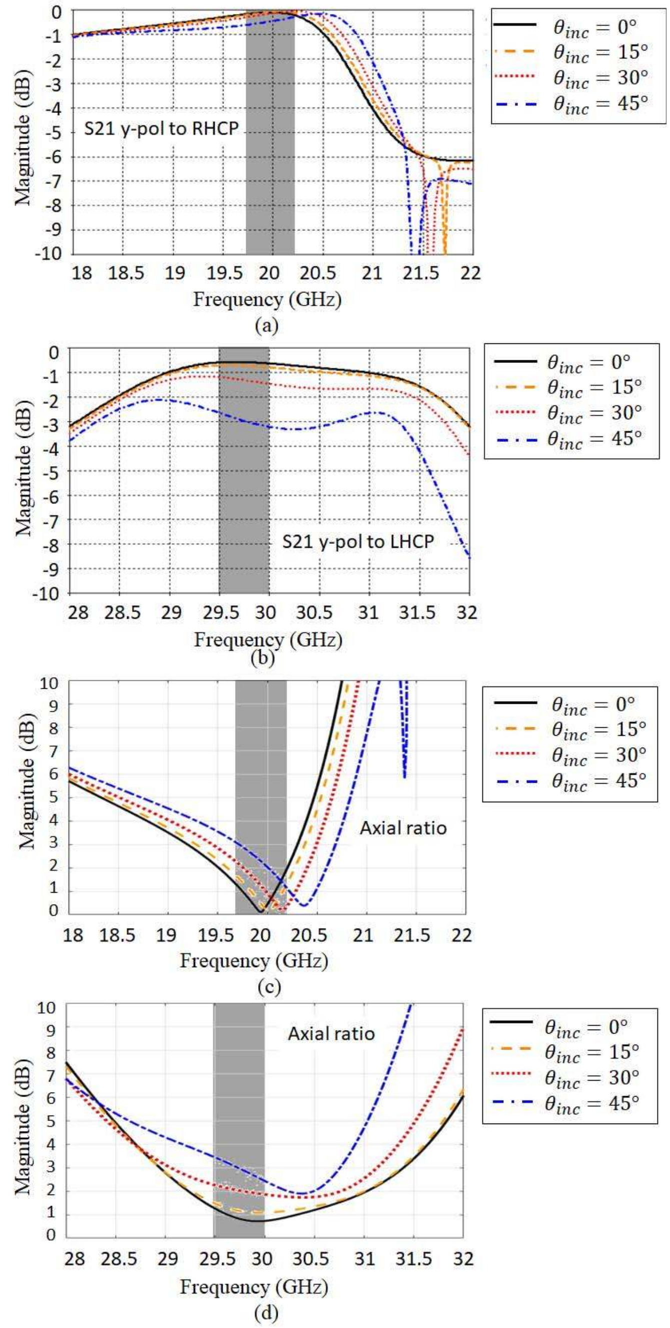

Fig. 6. Performance of the LP-to-CP cell for various incident angles at (a) and (c) lower frequency and (b) and (d) higher frequency bands. (a) y-polarized wave to RHCP transmission coefficient at the lower frequency band. (b) y-polarized wave to LHCP transmission coefficient at the higher frequency band. (c) Axial ratio at the lower frequency band. (d) Axial ratio at the higher frequency band.

However, in the measurements, we also tested $d = 21.3$ mm and $d = 23.7$ mm to find the best axial ratio and gain at both bands. Figs. 8 and 9 present the gain and axial ratio versus frequencies for the above d values, with the polarizer illuminated by the 20 and 30 GHz horns, respectively.

Fig. 8(a) confirms that the y-polarized wave from the horn gets mainly converted through the polarizer to RHCP wave in the lower band. Based on Fig. 8(a) and (b), while the RHCP gain does not change significantly for different

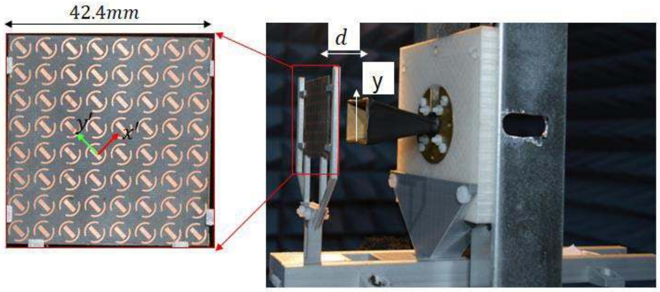

Fig. 7. 3-D printed setup to hold the horn and the polarizer.

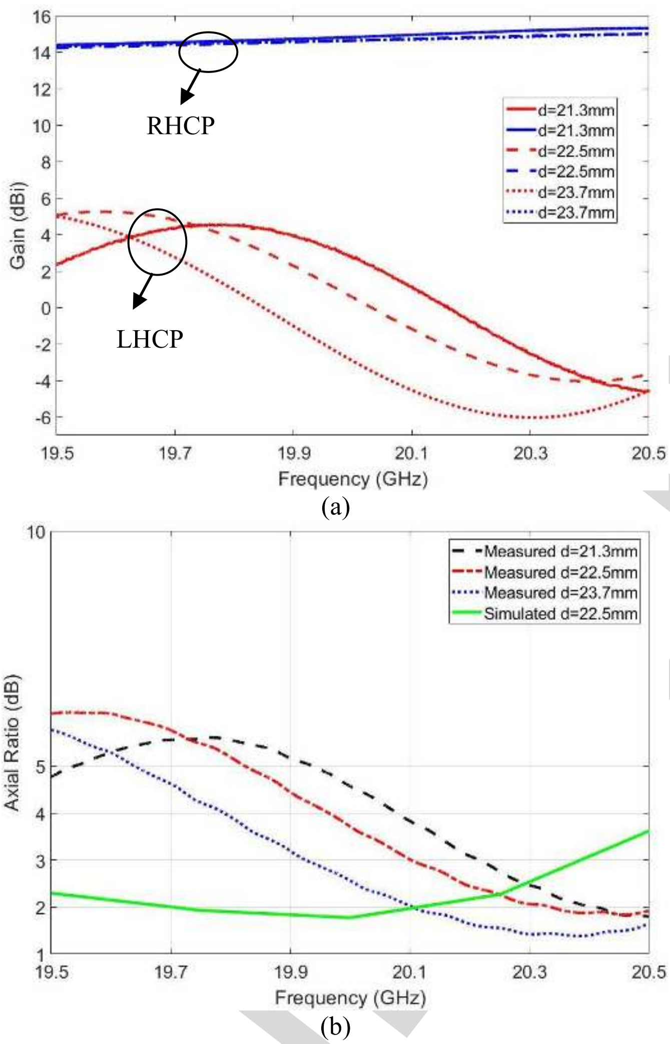

Fig. 8. (a) Measured CP gains and (b) simulated and measured axial ratio of the 20 GHz horn plus the polarizer at the higher band for different values of *d*.

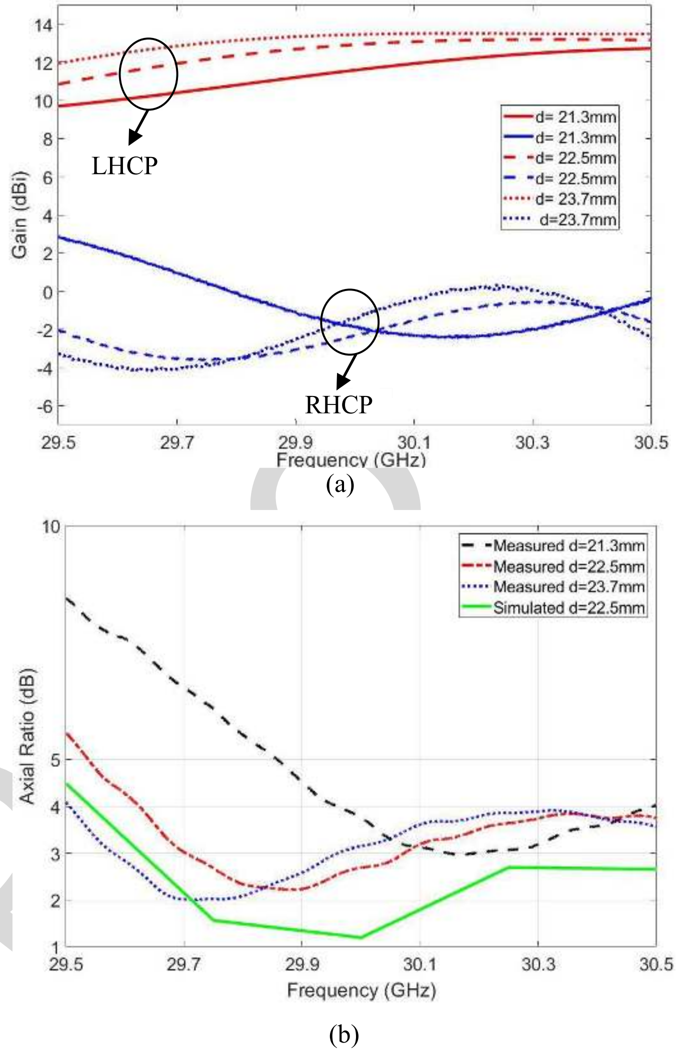

Fig. 9. (a) Measured CP gains and (b) simulated and measured axial ratio of the 30 GHz horn plus the polarizer at the higher band for different values of *d*.

values of d, the axial ratio is only 1.4 dB at 20.4 GHz for $d = 23.7$ mm. However, the value of d has to be optimized at both bands. Therefore, by looking at Fig. 9(a) and (b), it is obvious that $d = 23.7$ mm also maximizes the gain of LHCP wave at the higher band while it minimizes the gain of the cross RHCP. For this distance, the axial ratio of the 30 GHz horn and the polarizer has the minimum value of 2 dB at 29.7 GHz. Therefore, $d = 23.7$ mm was chosen for the rest of the measurements. It is worth mentioning that Figs. 8(a) and 9(a) confirm that the polarizer converts y-polarized incidence to RHCP at the lower band and LHCP at the higher band. Moreover, the bigger change in the values of the gain at the higher band stems from two reasons. First, the fact that any physical change in d is electrically larger at the higher band, and second, the reflection coefficient of the polarizer is larger at the higher band that causes more coupling between the aperture of the horn and the polarizer. The amount of this coupling changes with the change of d.

The CP radiation patterns of the polarizer in front of the 20 GHz horn when $d = 23.7$ mm are compared with the horn itself at 20 GHz in Fig. 10. Fig. 10 shows that the polarizer converts the y-polarized wave horn with low-insertion loss and cross-polarization level of 16 dB. Fig. 11 shows the comparison of the measured radiation pattern of the LP horn at 30 GHz with the CP patterns of the polarizer feed by the same horn. Fig. 11 shows the LP-to-CP conversion through the

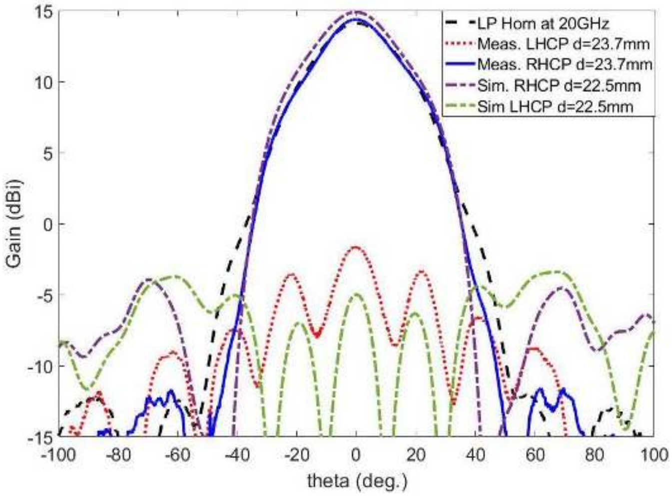

Fig. 10. Measured LP radiation pattern of the 20 GHz horn and simulated and measured CP patterns of the polarizer in front of the horn at, respectively, $d = 22.5$ mm and $d = 23.7$ mm at 20 GHz.

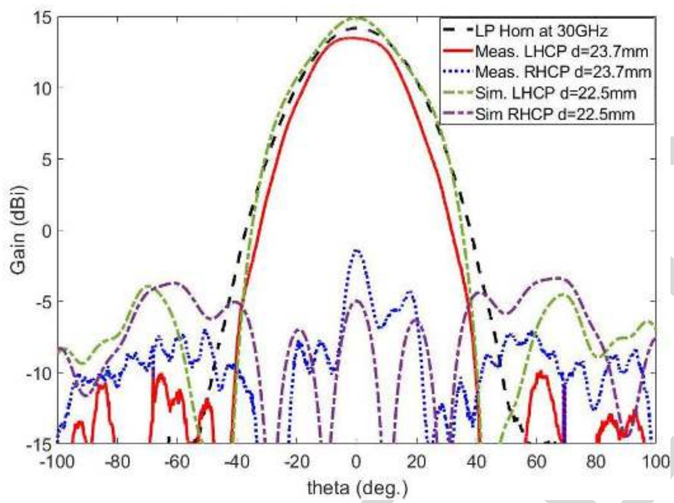

Fig. 11. Measured LP radiation pattern of the 30 GHz horn and simulated and measured CP patterns of the polarizer in front of the horn at, respectively, $d = 22.5$mm and $d = 23.7$mm at 30 GHz.

polarizer at 30 GHz occurs with only 0.7 dB insertion loss and 15 dB of cross-polarization level. Therefore, Figs. 10 and 11 confirm that the polarizer preserves the patterns of each horn and only convert its LP pattern to CP with minimum insertion loss.

The expansio
is explained ir
highlighted lin
horn plus the
plus the trans

ATION WITH A TRANSMIT-ARRAY FOR ND SATELLITE COMMUNICATIONS

I n, we employ the two standard gain LP rectangular horns working at 20 and 30 GHz plus the polarizer as feeds to illuminate a dual-band TA. We will onward call the whole combination of the horn, the polarizer, and the TA, HPTA. The measurements of the HPTA are done at 20.4 and 29.6 GHz based on the measurement results of Section IV and to obtain optimal value of axial ratio from the whole system. The dual-band TA used in this section is similar to the one proposed in [5], where the TA has an aperture size

AQ:6

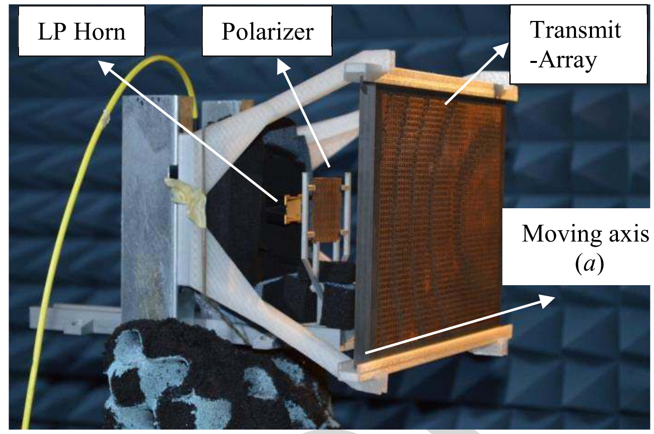

Fig. 12. 3-D printed setup to hold the LP horn, the polarizer, and the dual-band TA. The photograph shows that the setup allows the TA to be moved along the indicated displacement axis to steer the beam.

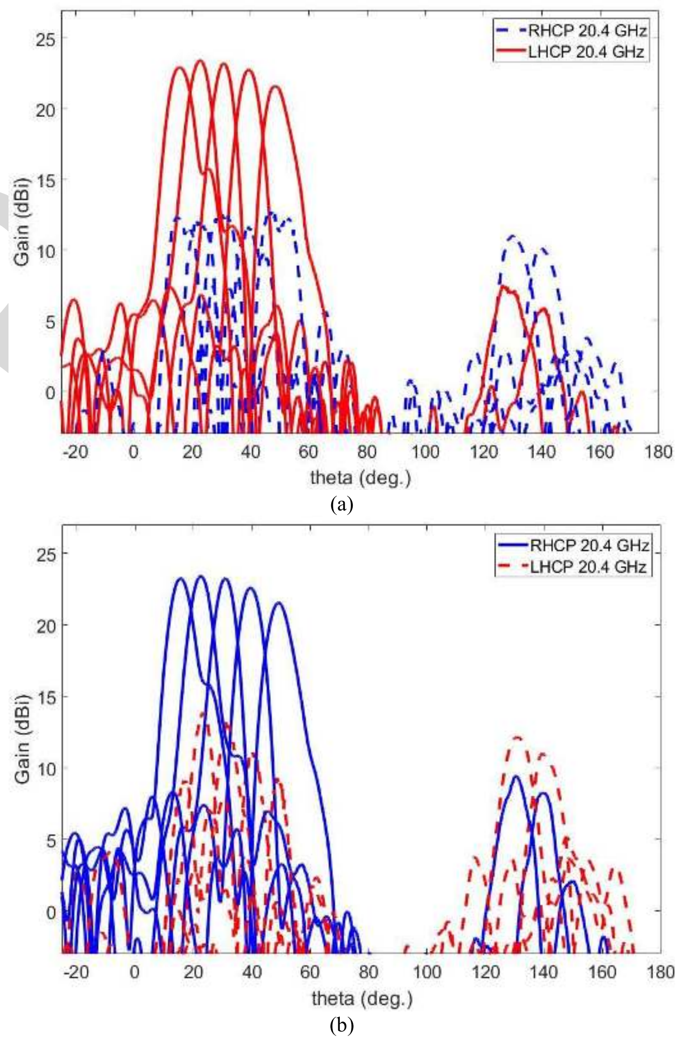

Fig. 13. CP radiation patterns of the 20.4 GHz horn plus the polarizer plus the TA when horn's radiation is (a) x-polarized and (b) y-polarized. Blue lines: RHCP patterns. Red lines: LHCP patterns.

of 196 mm × 147 mm. A 3-D printed support was used to hold the TA at a distance of $F = 100$ mm from the horn and in front of the polarizer. Fig. 12 shows the 3-D setup holding

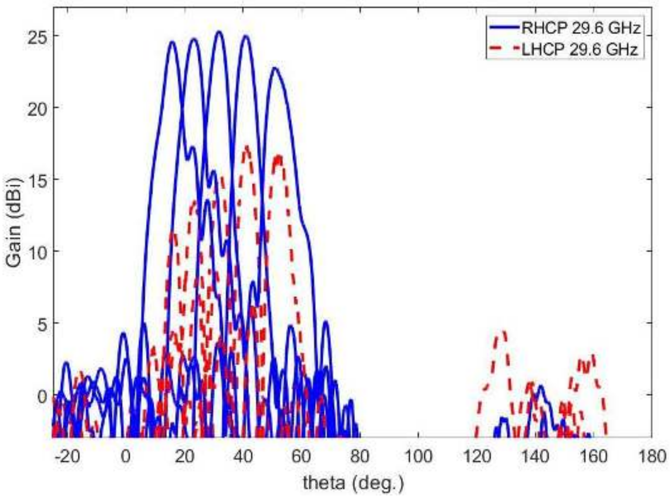

(a)

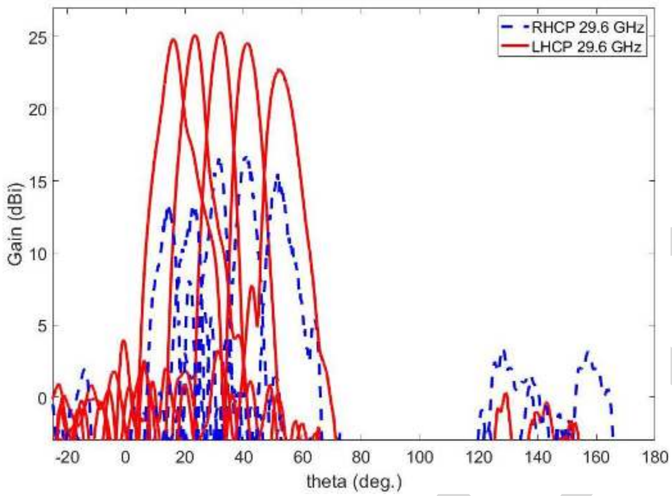

(b)

Fig. 14. CP radiation patterns of the 29.7 GHz horn plus the polarizer plus the TA when horn's radiation is (a) x-polarized and (b) y-polarized. Blue lines: RHCP patterns. Red lines: LHCP patterns.

TABLE II

SUMMARY OF THE PERFORMANCE OF THE HIGH-GAIN DUAL-BAND DUAL-CP ANTENNA COMPOSED OF THE HORN, THE POLARIZER, AND THE TA

20 GHz Horn							
LP	***a***	***Polarization***	***Gain (dBi)***	***Beam Direction***	***Scan Loss (dB)***	***X_{pol} (dB)***	***SLL(dB)***
***Polarizer* (Fig. 8)**							
y	0	RHCP	14.4	0º	---	-16	-23.5
***HPTA* (Fig. 13)**							
x	-15	LHCP	21.6	48.56º	-1.8	-8.8	-10.6
	0	LHCP	22.8	39.36º	-0.6	-11.3	-12.6
	15	LHCP	23.2	30.76º	-0.2	-10.7	-17.2
	30	LHCP	23.4	22.56º	0	-11.4	-20.4
	44	LHCP	23.0	15.65º	-0.4	-10.3	-19.2
y	-15	RHCP	21.6	49.06º	-1.8	-12.3	-9.7
	0	RHCP	22.6	39.46º	-0.8	-11.5	-11.6
	15	RHCP	23.2	30.96º	-0.2	-10.3	-16.1
	30	RHCP	23.4	22.56º	0	-9.7	-19.2
	44	RHCP	23.2	15.45º	-0.2	-13.2	-18.3
30 GHz Horn							
LP	***a***	***Polarization***	***Gain (dBi)***	***Beam Direction***	***Scan Loss (dB)***	***X_{pol} (dB)***	***SLL(dB)***
***Polarizer* (Fig. 9)**							
y	0	LHCP	13.5	0º	---	-15	-20.5
***HPTA* (Fig. 14)**							
x	-15	RHCP	22.8	50.96º	-2.5	-6.2	-17.8
	0	RHCP	25.0	40.86º	-0.3	-7.6	-22.6
	15	RHCP	25.3	31.86º	0	-10.1	-19.4
	30	RHCP	24.8	23.26º	-0.5	-11.3	-20.1
	44	RHCP	24.6	15.75º	-0.7	-13.1	-20.5
y	-15	LHCP	22.8	51.96º	-2.6	-8.1	-19.6
	0	LHCP	24.6	41.36º	-0.8	-8.0	-21.6
	15	LHCP	25.4	32.06º	0	-9.3	-23.4
	30	LHCP	25.2	23.36º	-0.2	-12.2	-22.9
	44	LHCP	24.9	16.05º	-0.5	-12.1	-21.2

each horn, the polarizer, and the dual-band TA at the designed distances from each other.

It can be seen from Fig. 12 that the TA can be moved along the shown displacement axis (a) to steer the beam. Here, we moved the TA from $a = -15$ mm to $a = 44$ mm, which corresponds to steering the beam from $\theta = 50°$ to $16°$ at 20 and 30 GHz in the zenith plane. The maximum of the beam is almost directed to the same angle at both frequencies with a difference less than 2°. Fig. 13(a) and (b) shows the CP radiation patterns of the horn, polarizer, and the TA at 20.4 GHz when the horn is x-polarized and y-polarized, respectively. We chose to measure the patterns at 20.4 GHz, since based on Fig. 8(b), the horn plus the polarizer provides minimum axial ratio of 1.4 dB at this frequency. At the end, it can be seen that for both the horn and its 90° rotated one, the HPTA provides maximum gain of 23.4 dBi and scanning loss of less than 1.8 dB in the scanning range of $16° - 50°$. The maximum cross-polarization levels when the horn is x-polarized or y-polarized are 11 and 10 dB, respectively. However, the cross-polarization level is dominated by the behavior of the TA, not only because of the intrinsic behavior of its UCs but also because of the demanding conditions for its operation with reduced F/D and wide-angle scanning. Improving the polarization discrimination of the aperture (TA or other), increasing F/D, and increasing the distance between the LP feed and the polarizer would lead to much lower cross-polarization levels, approaching those of the polarizer under plane-wave excitation. It is worth noticing that orthogonal LP incident waves, here, are obtained by rotating the horn by 90°. However, the same results can be obtained by rotating the polarizer by 90°. Moreover, employing a dual-LP feed eliminates the need for this step.

After measuring the HPTA at the lower band, we replaced the 20 GHz horn with the 30 GHz horn in the 3-D printed support (Fig. 12). Based on both the gain and the axial ratio of the 30 GHz horn with the polarizer (Fig. 9), we performed the measurements at 29.6 GHz, where the gain is 15.8 dBi and the axial ratio is 2.8 dB. Fig. 14(a) shows the CP radiation patterns when the horn is radiating x-polarized wave, and Fig. 14(b) shows the radiation patterns when the horn is 90° rotated. We again moved the TA along a-axis from $a = -15$ mm to $a = 44$ mm to steer the beam at 29.6 GHz. This corresponds to steering the beam from $\theta = 50°$ to $16°$ with maximum gain of 25.3 dBi and scanning loss of 2.5 dB at 29.6 GHz. The maximum cross-polarization level is 8 dB due to the performance of the TA's elements at this frequency. Finally, Table II summarizes the performance of the HPTA for all the a-positions of the TA with respect to the 20 and 30 GHz horns for both LP radiations.

VI. Conclusion

The possibility of using a single aperture to produce dual-band dual-CP beams, capable of fast toggling of the polarization sense, is very much desired, especially for satellite communications. In this paper, the design complexity of such a primary feed is lowered by using a separate LP feed and a novel passive LP-to-CP polarizer. The proposed polarizer is the focus of this paper. It operates in the transmission mode at two separate nonadjacent frequency bands, converting each orthogonal LP incident waves into orthogonal outgoing CP waves at the two frequency bands. This unique feature of the polarizer allows toggling the polarization sense between the uplink and downlink bands just by switching between two orthogonal incident LP waves. This fulfills completely the above-mentioned requirement in the beginning of the paragraph.

In order to isolate the behavior of the polarizer, in this paper, we used 20 and 30 GHz horns to generate very pure LP incident fields. It was shown that the polarizer reasonably preserves the radiation pattern of the horn while it changes the polarization of the outgoing wave as required. To assess the usefulness of the proposed concept, the horn-plus-polarizer assembly was successfully used to illuminate a K/Ka dual-band TA with CP and wide-angle beam steering.

The separate structure of the primary feed allows great flexibility to use the polarizer in different conditions. For instance, a low-profile printed technology switched dual-LP feed can be used with the same polarizer, instead of the horns. The polarizer can be redesigned for any desired frequency bands and employed separately for various applications. For example, the polarizer itself can be placed in close distance from a dual-band LP reflect array and convert it to dual-band dual-CP reflect array similar to the work done for a single-band RA [32] but for dual-band operation.

Acknowledgment

The authors would like to thank the collaboration from C. Brito and J. Felício for prototype construction. They would like to thank A. Almeida for prototype construction and measurements because without his meticulous work and great patience, implementation of this project was not possible. They would like to thank Rogers Corporation for donating substrates used for the prototypes. They would also like to thank the Instituto de Plasmas e Fusão Nuclear from Instituto Superior Técnico, University of Lisbon, Lisbon, Portugal, for sharing computational resources.

References

[1] S. Gao, Q. Luo, and F. Zhu, "Introduction to circularly polarized antennas," in *Circularly Polarized Antennas*. London, U.K.: Wiley, 2014, pp. 1–25.

[2] R. Garcia, F. Mayol, J. M. Montero, and A. Culebras, "Circular polarization feed with dual-frequency OMT-based turnstile junction," *IEEE Antennas Propag. Mag.*, vol. 53, no. 1, pp. 226–236, Feb. 2011.

[3] C. A. Leal-Sevillano, J. A. Ruiz-Cruz, J. R. Montejo-Garai, and J. M. Rebollar, "Novel dual-band single circular polarization antenna feeding network for satellite communications," in *Proc. 8th Eur. Conf. Antennas Propag. (EuCAP)*, Apr. 2014, pp. 3265–3269.

[4] E. B. Lima, S. A. Matos, J. R. Costa, C. A. Fernandes, and N. J. G. Fonseca, "Circular polarization wide-angle beam steering at Ka-band by in-plane translation of a plate lens antenna," *IEEE Trans. Antennas Propag.*, vol. 63, no. 12, pp. 5443–5455, Dec. 2015.

[5] S. A. Matos *et al.*, "High gain dual-band beam steering transmitarray for satcom terminals at ka band," *IEEE Trans. Antennas Propag.*, vol. 65, no. 7, pp. 3528–3539, Jul. 2017.

[6] S. Ye *et al.*, "High-gain planar antenna arrays for mobile satellite communications [antenna applications corner]," *IEEE Antennas Propag. Mag.*, vol. 54, no. 6, pp. 256–268, Dec. 2012.

[7] S. Hebib, H. Aubert, O. Pascal, N. J. G. Fonseca, L. Ries, and J. M. E. Lopez, "Multiband pyramidal antenna loaded with a cutoff open-ended waveguide," *IEEE Trans. Antennas Propag.*, vol. 57, no. 1, pp. 266–270, Jan. 2009.

[8] S. D. Targonski, R. B. Waterhouse, and D. M. Pozar, "Design of wide-band aperture-stacked patch microstrip antennas," *IEEE Trans. Antennas Propag.*, vol. 46, no. 9, pp. 1245–1251, Sep. 1998.

[9] Z. Yang and K. F. Warnick, "Multiband dual-polarization high-efficiency array feed for Ku/reverse-band satellite communications," *IEEE Antennas Wireless Propag. Lett.*, vol. 13, pp. 1325–1328, 2014.

[10] A. D. Olver, P. J. B. Clarricoats, and A. A. Kishk, *Microwave Horns and Feeds*. New York, NY, USA: Institution of Electrical Engineers, 1994.

[11] F. F. Manzillo, M. Ettorre, R. Sauleau, and A. Grbic, "Systematic design of a class of wideband circular polarizers using dispersion engineering," in *Proc. 11th Eur. Conf. Antennas Propag. (EUCAP)*, Davos, Switzerland, Mar. 2017, pp. 1279–1281.

[12] S. M. A. M. H. Abadi and N. Behdad, "Wideband linear-to-circular polarization converters based on miniaturized-element frequency selective surfaces," *IEEE Trans. Antennas Propag.*, vol. 64, no. 2, pp. 525–534, Feb. 2016.

[13] L. Martinez-Lopez, J. Rodriguez-Cuevas, J. I. Martinez-Lopez, and A. E. Martynyuk, "A multilayer circular polarizer based on bisected split-ring frequency selective surfaces," *IEEE Antennas Wireless Propag. Lett.*, vol. 13, pp. 153–156, 2014.

[14] M. Euler, V. Fusco, R. Cahill, and R. Dickie, "325 GHz single layer sub-millimeter wave FSS based split slot ring linear to circular polarization convertor," *IEEE Trans. Antennas Propag.*, vol. 58, no. 7, pp. 2457–2459, Jul. 2010.

[15] M.-A. Joyal and J.-J. Laurin, "Analysis and design of thin circular polarizers based on meander lines," *IEEE Trans. Antennas Propag.*, vol. 60, no. 6, pp. 3007–3011, Jun. 2012.

[16] I. Sohail, Y. Ranga, K. P. Esselle, and S. G. Hay, "A linear to circular polarization converter based on Jerusalem-cross frequency selective surface," in *Proc. 7th Eur. Conf. Antennas Propag. (EuCAP)*, Apr. 2013, pp. 2141–2143.

[17] W. Li *et al.*, "A reconfigurable polarization converter using active metasurface and its application in horn antenna," *IEEE Trans. Antennas Propag.*, vol. 64, no. 12, pp. 5281–5290, Dec. 2016.

[18] H. L. Zhu, S. W. Cheung, K. L. Chung, and T. I. Yuk, "Linear-to-circular polarization conversion using metasurface," *IEEE Trans. Antennas Propag.*, vol. 61, no. 9, pp. 4615–4623, Sep. 2013.

[19] M. Mutlu, A. E. Akosman, A. E. Serebryannikov, and E. Ozbay, "Asymmetric chiral metamaterial circular polarizer based on four U-shaped split ring resonators," *Opt. Lett.*, vol. 36, no. 9, pp. 1653–1655, May 2011.

[20] N. J. G. Fonseca and C. Mangenot, "Low-profile polarizing surface with dual-band operation in orthogonal polarizations for broadband satellite applications," in *Proc. 8th Eur. Conf. Antennas Propag. (EuCAP)*, The Hague, The Netherlands, Apr. 2014, pp. 570–574.

[21] N. J. G. Fonseca and C. Mangenot, "High-performance electrically thin dual-band polarizing reflective surface for broadband satellite applications," *IEEE Trans. Antennas Propag.*, vol. 64, no. 2, pp. 640–649, Feb. 2016.

[22] W. Tang, S. Mercader-Pellicer, G. Goussetis, H. Legay, and N. J. G. Fonseca, "Low-profile compact dual-band unit cell for polarizing surfaces operating in orthogonal polarizations," *IEEE Trans. Antennas Propag.*, vol. 65, no. 3, pp. 1472–1477, Mar. 2017.

[23] A. Abbaspour-Tamijani, K. Sarabandi, and G. M. Rebeiz, "Antenna-filter-antenna arrays as a class of bandpass frequency-selective surfaces," *IEEE Trans. Microw. Theory Techn.*, vol. 52, no. 8, pp. 1781–1789, Aug. 2004.

[24] T. Chaloun, V. Ziegler, and W. Menzel, "Design of a dual-polarized stacked patch antenna for wide-angle scanning reflectarrays," *IEEE Trans. Antennas Propag.*, vol. 64, no. 8, pp. 3380–3390, Aug. 2016.

[25] P. Naseri, F. Khosravi, and P. Mousavi, "Antenna-filter-antenna-based transmit-array for circular polarization application," *IEEE Antennas Wireless Propag. Lett.*, vol. 16, pp. 1389–1392, 2017.

[26] P. Naseri, R. Mirzavand, and P. Mousavi, "Dual-band circularly polarized transmit-array unit-cell at X and K bands," in *Proc. 10th Eur. Conf. Antennas Propag. (EuCAP)*, Davos, Switzerland, Apr. 2016, pp. 1–4.

[27] P. Naseri, C. A. Fernandes, S. A. Matos, and J. R. Costa, "Antenna-filter-antenna-based cell for linear-to-circular polarizer transmit-array," in *Proc. APS*, San Diego, CA, USA, Jul. 2017, pp. 1071–1072.

[28] P. Naseri, S. A. Matos, J. R. Costa, and C. A. Fernandes, "Phase-delay versus phase-rotation cells for circular polarization transmit arrays—Application to satellite Ka-band beam steering," *IEEE Trans. Antennas Propag.*, vol. 66, no. 3, pp. 1236–1247, Mar. 2018.

[29] CST Microwave Studio. (Oct. 2014). *Computer Simulation Technology*. [Online]. Available: http://www.cst.com

[30] R. Pous and D. M. Pozar, "A frequency-selective surface using aperture-coupled microstrip patches," *IEEE Trans. Antennas Propag.*, vol. 39, no. 12, pp. 1763–1769, Dec. 1991.

[31] S. A. Matos, E. B. Lima, J. R. Costa, C. A. Fernandes, and N. Fonseca, "Experimental evaluation of a high gain dual-band beam steerable transmit-array," ~~in Proc.~~ *12th Eur. Conf. Antennas Propag. (EuCAP)*, London, U.K., Apr. 2018.

To be pu

AQ:8

[32] M. Hosseini and S. V. Hum, "A dual-CP reflectarray unit cell for realizing independently controlled beams for space applications," in *Proc. 11th Eur. Conf. Antennas Propag. (EuCAP)*, Paris, France, Mar. 2017, pp. 66–70.

Parinaz Naseri (M'14) received the B.Sc. degree in electrical engineering (telecommunications) from the University of Tehran, Tehran, Iran, in 2013, and the M.Sc. degree in electromagnetics and microwaves, electrical engineering from the University of Alberta, Edmonton, AB, Canada, in 2017.

From 2016 to 2017, she was a Grant Researcher with the Instituto de Telecomunicações, Lisbon, Portugal. Since 2018, she has been a Researcher with the Reconfigurable Antenna Laboratory, University of Toronto, Toronto, ON, Canada. She has received the Stanley G. Jones Master's Scholarship in 2014 and the Ontario Trillium Scholarship toward her Ph.D. program at the University of Toronto in 2018. Her current research interests include frequency selective surfaces, transmit arrays, reflectarrays, and polarimetric surfaces.

Sérgio A. Matos (S'05–M'16) received the Licenciado, M.Sc., and Ph.D. degrees in electrical and computer engineering from the Instituto Superior Técnico, University of Lisbon, Lisbon, Portugal, in 2004, 2005, and 2010, respectively.

He is currently a Researcher with the Instituto de Telecomunicações, Lisbon. He is also an Assistant Professor with the Departamento de Ciências e Tecnologias da Informação, Instituto Universitário de Lisboa, Lisbon. He has co-authored 60 technical papers in international journals and conference proceedings. His current research interests include electromagnetic wave propagation in metamaterials, flat-lens design, and transmit arrays.

Jorge R. Costa (S'97–M'03–SM'09) was born in Lisbon, Portugal, in 1974. He received the Licenciado and Ph.D. degrees in electrical and computer engineering from the Instituto Superior Técnico, Technical University of Lisbon, Lisbon, Portugal, in 1997 and 2002, respectively.

He is currently a Researcher with the Instituto de Telecomunicações, Lisbon. He is also an Associate Professor with the Departamento de Ciências e Tecnologias da Informação, Instituto Universitário de Lisboa, Lisbon. He has co-authored four patent applications and more than 150 contributions to peer-reviewed journals and international conference proceedings. More than 30 of these papers have appeared in the IEEE JOURNALS. His current research interests include lenses, reconfigurable antennas, MEMS switches, UWB, MIMO, and RFID antennas.

Dr. Costa served as an Associate Editor for the IEEE TRANSACTIONS ON ANTENNAS AND PROPAGATION from 2010 to 2016. He was a Guest Editor of the Special Issue on *Antennas and Propagation at MM- and Sub MM-Waves* from the IEEE TRANSACTIONS ON ANTENNAS AND PROPAGATION, in 2013. He was the Co-Chair of the Technical Program Committee of the European Conference on Antennas and Propagation (EuCAP 2015) in Lisbon and the General Vice-Chair of EuCAP 2017 in Paris.

Carlos A. Fernandes (S'86–M'89–SM'08) received the Licenciado, M.Sc., and Ph.D. degrees in electrical and computer engineering from the Instituto Superior Técnico (IST), Technical University of Lisbon, Lisbon, Portugal, in 1980, 1985, and 1990, respectively.

In 1980, he joined IST, where he is currently a Full Professor of microwaves, radio wave propagation, and antennas with the Department of Electrical and Computer Engineering. He is currently a Senior Researcher with the Instituto de Telecomunicações, Lisbon, Portugal. He has co-authored over a book, two book chapters, and 180 technical papers in peer-reviewed international journals and conference proceedings. He holds seven patents in the areas of antennas and radiowave propagation modeling. His current research interests include dielectric antennas for millimeter-wave applications, antennas and propagation modeling for personal communication systems, RFID and UWB antennas, artificial dielectrics, and metamaterials.

Dr. Fernandes was a member of the Board of Directors. He was a Guest Editor of the Special Issue on *Antennas and Propagation at MM- and Sub MM-Waves* ... ND PROPAGATION, in 2 ...

~~He was an Anten ... Alcatel Alénia Spac ... the Antennas Sectio ... the Antenna and S ... Noordwijk, The Net ... in journals, confer ... 18 technical innovat ... current research inte ... beam formers theor ... metamaterials.~~

~~Dr. Fonseca was ... Engineer Paper Awa ... is currently serving ... the IEEE TRANSAC ... TRANSACTIONS ON~~

Please update to:
He works in the Antenna and Sub-Millimetre Section, European Space Agency (ESA), N Netherlands, since 2009. His current resear include multiple beam antennas for space m beam-formers theory and design, user termi and novel manufacturing techniques. He ha co-authored more than 170 papers in peer-r journals and conferences. He contributed to innovations, protected by over 40 patents is pending.
Dr. Fonseca is serving or served as a TPC r several conferences, chaired the 38th ESA workshop on Innovative Antenna Systems a Technologies for Future Space Missions, O and co-chaired the 2018 IET Loughborough Propagation conference (LAPC 2018). He is technical reviewer for several journals, inclu Transactions on Antennas and Propagation IEEE Transactions on Microwave Theory ar (TMTT). He received several prizes and aw ESA Technical Improvement Awards in 201 He was the recipient of the IEEE Antennas a Propagation Society Commendation Certific recognizing the exceptional performance of the IEEE Transactions on Antennas and Pr 2016.

AUTHOR QUERIES

PLEASE NOTE: We cannot accept new source files as corrections for your paper. If possible, please annotate the PDF proof we have sent you with your corrections and upload it via the Author Gateway. Alternatively, you may send us your corrections in list format. You may also upload revised graphics via the Author Gateway.

AQ:1 = Author: Please confirm or add details for any funding or financial support for the research of this article.
AQ:2 = Please note that current affiliation for "Parinaz Naseri" does not match from the F.F. to the bio. Please check and confirm.
AQ:3 = Please confirm whether the authors affiliation details are correct as set.
AQ:4 = Please confirm whether the edits made in this part "therefore, it is a very good…" retains the intended meaning.
AQ:5 = Please provide the subpart description for Fig. 5.
AQ:6 = Please provide an expansion for "HPTA."
AQ:7 = Please provide location for "Rogers Corporation."
AQ:8 = Please provide the page range for ref. [31].

Dual-Band Dual-Linear-to-Circular Polarization Converter in Transmission Mode Application to *K*/*Ka*-Band Satellite Communications

Parinaz Naseri, *Member, IEEE*, Sérgio A. Matos, *Member, IEEE*, Jorge R. Costa, *Senior Member, IEEE*, Carlos A. Fernandes, *Senior Member, IEEE*, and Nelson J. G. Fonseca, *Senior Member, IEEE*

***Abstract*— Many wireless communication applications such as satellite communications use circularly polarized (CP) signals, with the requirement for easy switching of the polarization sense between uplink and downlink. Specifically, in satellite communications, the trend is also to move to higher frequencies and integrate the receiving and transmitting antennas in one dual-band terminal. However, these simultaneous demands make the design and fabrication of the composing parts very challenging. We propose, here, a dual-band dual-linear polarization (LP)-to-CP converter that works in the transmission mode. The working principle of this polarizer is explained through an example for Ka-band satellite communications at 19.7–20.2 and 29.5–30 GHz. The LP-to-CP converter is a single panel composed of identical unit cells with a thickness of only 1.05 mm and a size of 5.3 mm × 5.3 mm. Due to its operation in the transmission mode, the polarizer can be combined with a simple dual-band dual-LP antenna to obtain the desired dual-band dual-CP single antenna. However, the unique property of this polarizer is yet the fact that it converts a given LP wave, e.g., x-polarization, to orthogonal CP waves at the two nonadjacent frequency bands, e.g., left-handed CP at lower band and right-handed CP at higher band. The polarizer is tested both with 20 and 30 GHz LP rectangular horns to illuminate a dual-band transmit array (TA) to obtain wide-angle steering of CP beams. The performance of the polarizer and its association with the TA is evaluated through simulation and measurements. We also present design guidelines for this type of polarizer.**

***Index Terms*— Antenna–filter–antenna, circular polarization (CP), dual-band antennas, frequency selective surfaces, periodic structures, polarization conversion.**

AQ:1 Manuscript received May 3, 2018; revised July 21, 2018; accepted October 4, 2018. This work was supported in part by the European Space Agency under Contract 4000109111/13/NL/AD and in part by the Fundação para a Ciência e Tecnologia under Project PEstOE/EEI/LA/0008/2013 and Project UID/EEA/50008/2013. *(Corresponding author: Parinaz Naseri.)*

AQ:2 P. Naseri and C. A. Fernandes are with the Instituto de Telecomunicações, 1049-001 Lisbon, Portugal, and also with the Instituto Superior Técnico, Universidade de Lisboa, 1049-001 Lisbon, Portugal (e-mail: parinaz.naseri@lx.it.pt).

AQ:3 S. A. Matos and J. R. Costa are with the Instituto de Telecomunicações, 1049-001 Lisbon, Portugal, with the Instituto Superior Técnico, Universidade de Lisboa, 1049-001 Lisbon, Portugal, and also with the Departamento de Ciências e Tecnologias da Informação, Instituto Universitário de Lisbon, 1649-026 Lisbon, Portugal.

N. J. G. Fonseca is with the Antenna and Sub-Millimetre Wave Section, European Space Agency, 2200 AG Noordwijk, The Netherlands (e-mail: nelson.fonseca@esa.int).

Color versions of one or more of the figures in this paper are available online at http://ieeexplore.ieee.org.

Digital Object Identifier 10.1109/TAP.2018.2874680

I. Introduction

In SOME applications such as satellite and point-to-multipoint communications, circular polarization (CP) is preferred over linearly polarized (LP) radiation because it is less influenced by multipath fading and by polarization mismatch associated with ground terminal mobility [1].

For satellite communications (satcom), besides CP, an antenna is usually required to operate at two distinct and nonadjacent frequency bands in orthogonal polarizations as a means to further enhance the isolation between transmit and receive signals, as power flux densities for those types of applications are very low and particularly sensitive to interference. For example, broadband satellite communications at *Ka*-band make use of a dedicated frequency spectrum with the downlink (D/L) at 19.7–20.2 GHz and the uplink (U/L) at 29.5–30 GHz. If the user (ground) terminal receives (D/L) a left-handed CP (LHCP) electromagnetic (EM) field, it should transmit (U/L) an orthogonal EM field, in this case, a right-handed CP (RHCP) field. Another important aspect for mobile satcom applications associated with spot beam broadband satellites is the polarization diversity over the service area, meaning that the user terminal must be able to switch from one polarization to another in both bands, while maintaining the polarization orthogonality between the two bands when doing the handover between one spot and the adjacent one.

In order to respond to these requirements, user terminal antennas for *Ka*-band satcom often use a horn antenna combined with an orthomode transducer to feed a reflector [2], [3] or transmit array (TA) [4], [5]. Alternatively, the terminal antenna may be a phased array of dual-band dual-CP patch antennas [6]–[9]. However, these solutions are either bulky and expensive or compact but inefficient and hard to fabricate at *Ka*-band frequencies. There is a demand for simpler solutions, low profile, low cost, and easy to fabricate up to millimeter-wave frequencies. In general, CP waves can be generated by antennas such as the truncated microstrip patch, crossed dipoles [6], helix, and spiral [1]. However, none of these allows dual band, unidirectional radiation patterns with moderate directivity (e.g., 10–20 dBi) in a simple implementation without the need for a polarization device, typically a hybrid directional coupler.

The literature offers another way of generating CP EM fields by combining an LP antenna and a polarization converter to avoid the above-mentioned shortcomings of conventional CP antennas. The polarization converter is basically an anisotropic medium that fully transmits (or reflects) a given LP field with a 90° phase difference along its two main axes, orthogonal to the direction of propagation. Hence, an incoming slant LP field, i.e., at 45° with respect to the two main axes, will be converted into a CP field. This sort of medium has been generally implemented using existing materials and various different metallic element designs in planar periodic structures such as frequency selective surfaces [11]–[16] and metasurfaces [17]–[19]. The existing LPs-to-CPs are mostly either wideband [11]–[13] or single band [14]–[18]. In [19], a very interesting polarizer based on a chiral cell geometry is used to convert an incident LP wave into orthogonal handedness CP waves in a low band and a high band. However, it only works for x-LP incident wave, imposing a fixed CP handedness at the low and high bands. This precludes the use of this type of cell for mobile satellite applications requiring polarization switching for handover purposes as described earlier. In [20], a polarization converter in the reflection mode was introduced, having a dual-band dual-polarization capability with the desired polarization orthogonality between the two separate operating bands from the same incident LP field. This characteristic, considered for the space segment in [20]–[22], is demonstrated here with a polarization converter in transmission mode for the ground segment, and more specifically user terminals. Using a TA instead of a polarizing reflector design allows for reduced antenna height, which is desirable for mobile user terminal applications. In addition, the dual-band dual-polarization characteristic would enable the design of a TA antenna with a simplified feed design, either a single-polarized feed, eventually rotating 90° for handover purposes, or a dual-polarized feed combined with a single-wideband switch, also for handover purposes.

This paper focuses on a new compact and efficient dual-band dual-CP that can be used to create an antenna satisfying all the previously identified aperture-feeding requirements for user terminals in multispot satellite communication systems. In fact, we propose a novel and low-loss dual-band dual-LP-to-CP converter to be operated in combination with a simple dual-band dual-LP feed antenna. We demonstrate the performance of the polarizer fed by an LP horn to illuminate a high-gain dual-band wide-angle beam steering TA. Together they form a low-profile dual-band dual-CP user terminal antenna for *Ka*-band satellite communications. We further present design rules for the polarizer.

This paper is organized as follows. In Section II, different components of the overall proposed antenna are presented and described. In Section III, the unit cell (UC) of the LP-to-CP converter is introduced and the effects of different physical parameters on the frequency response of the UC are explained. Section IV presents the simulation and measurement results of two horns at 20 and 30 GHz combined with the polarization converter. Finally, in Section V, the combinations of the horns and the polarizer are employed to feed a dual-band TA to implement a low-profile dual-band dual-CP ground terminal for *Ka*-band satellite communication.

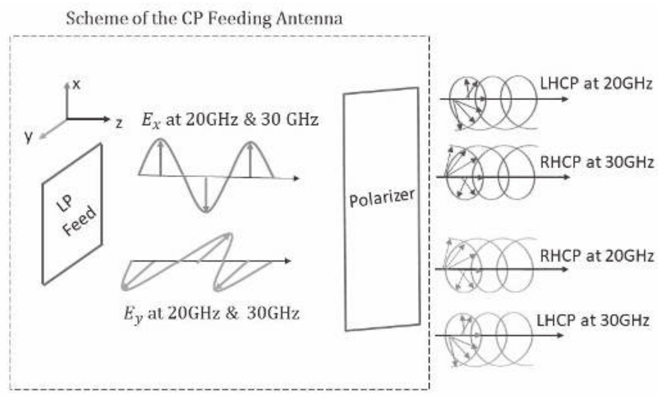

Fig. 1. Scheme of the dual-band dual-CP antenna to feed a large aperture for *Ka*-band satellite communications. It is composed of the dual-band LP feed and a dual-band LP-to-CP.

II. Antenna Configuration

Fig. 1 shows the scheme of the proposed dual-band dual-CP antenna to feed a large aperture for *Ka*-band satellite communications. The feed element excites two orthogonal LPs at two frequency bands. Each LP illuminates the polarizer and gets converted to two orthogonal CPs at the two frequency bands. Note that, for the same input LP, the output CP is orthogonal between the U/L and D/L bands. The design of a dual-band linear antenna to feed the polarizer is out of the goals of this paper. Therefore, in this paper and as a proof-of-concept, the LP waves at 20 and 30 GHz are radiated by two LP rectangular horns operating at these respective frequencies.

The proposed LP-to-CP converter is a single panel composed of identical UCs. These elements have dual-band operation with the low insertion loss at both bands. Besides, the polarizer is physically and electrically very thin (only 1.05 mm, corresponding to $0.07\lambda_0$ and $0.11\lambda_0$ at 20 and 30 GHz, respectively).

The working principle of the polarizer starts with the splitting of an LP wave into two orthogonal linear components, like standard polarization converters do. However, it then generates −90° phase shift between them at the lower frequency band and +90° phase shift at the higher frequency band. This means that a linear x-polarized incident wave at the lower frequency band gets converted to an LHCP wave through the polarizer, while the same LP wave gets converted to an RHCP wave at the higher frequency band. The polarizer functions the same way for a linear y-polarized incident wave, but it converts into the orthogonal CP wave at each band compared to the x-polarized incidence.

III. Linear-to-Circular Polarizer Unit Cell

The UCs that compose the proposed LP-to-CP converter present x'- and y'-axes symmetries [$x'y'z'$ is the local coordinate system of the cell, rotated 45° around the z-axis with respect to the main xyz coordinate system, see Fig. 2(a)], and are similar to the ones introduced in [25]–[28].

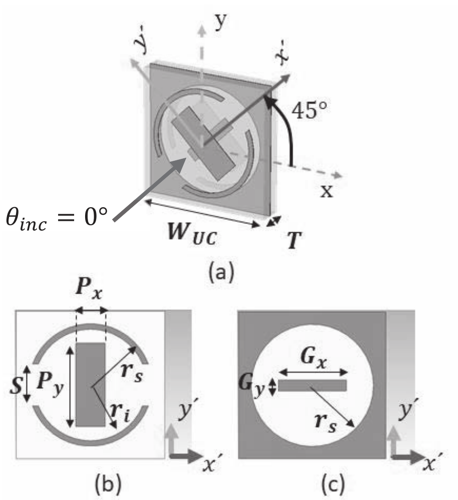

Fig. 2. Structure of the UC. (a) 3-D view. (b) First layer. (c) Second layer.

Once an LP incident wave makes a ±45° angle in relation to the x'- and y'-axes of the cell [Fig. 2(a)], the cell decomposes the wave into two orthogonal components along x'- and y'-axes. To avoid generating a +45° directed incident wave, we rotated the cell by 45°. Then, it transmits both components with almost equal amplitude and −90° phase difference at 20 GHz and +90° phase difference at 30 GHz. For example, the +45°-rotated UC converts a y-polarized incident wave to an RHCP at 20 GHz and to an LHCP at 30 GHz through the polarizer.

The cell is composed of three metallic layers parallel to the $x'y'$ plane, separated by thin 0.508 mm dielectric Rogers DuroidTM 5880 slabs ($\varepsilon_r = 2.2$ and $tan\delta = 0.0009$). The first and the third layers of the UC are identical and composed of a patch and a split ring. The middle layer is composed of a circular slot plus a rectangular patch.

Due to the asymmetric elements along x'- and y'-axes (lack of 90° rotational symmetry), the UC responds differently to the two orthogonal LP and normal incident waves (i.e., x′-polarized and y′-polarized waves). To operate as an LP-to-CP converter, the cell should transmit both x'- and y'-polarized waves with equal amplitude and 90° phase difference. The proposed UC shown in Fig. 2 provides this distinct response to x'- and y'-polarized normal incidences at two frequency bands.

The design and optimization of this UC were performed in CST Microwave Studio [29] using periodic boundary conditions in x'- and y'-directions and open in z'-direction so that it operates at dual-satellite communication *Ka*-band, i.e., 19.7–20.2 and 29.5–30 GHz. The structure is illuminated by two normal plane waves propagating in the z'-direction with the electric fields in x'- and y'-directions. The optimization aimed to obtain linear reflection coefficients below −10 dB; therefore, it is a very good transmission, while the phase difference between the two linear transmission coefficients was required to be about ±90° at both frequency bands. The optimized dimensions of the cell are summarized in Table I. The reflection coefficients of the UC for these normal incident

TABLE I
DIMENSIONS OF THE UC

parameter	length (mm)	parameter	length (mm)
G_x	2.35	r_s	2.2
G_y	0.5	S	1.5
P_x	0.9	T	1.05
P_y	2.9	w_{UC}	5.3
r_i	1.85		

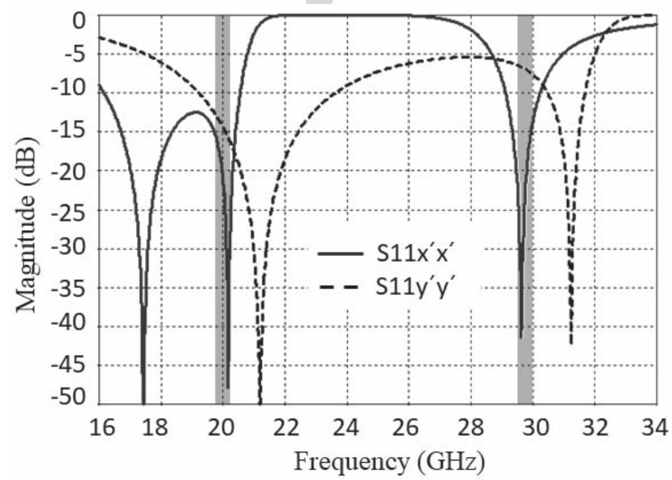

Fig. 3. Reflection coefficients of the UC for an x′-polarized and a y′-polarized normal incident waves.

waves are presented in Fig. 3. The gray bars in Fig. 3 highlight the two frequency bands of the dual-*Ka*-band satellite communications. Fig. 4(a) and (b) shows the amplitude and phase of the transmission coefficients of the cell for these orthogonal incidences. Based on these much different coefficients of the cell, it can be concluded that the cell presents distinct features to the x'- and y'-polarized waves.

A. Cell Design Guidelines

To design a similar cell for other frequencies, one should choose W_{UC} close to $\lambda/2$, where λ is the wavelength at the higher frequency band. It is also essential that the behavior of the reflection coefficients of the cell follows the one depicted in Fig. 3, where the first two resonances of the cell to an x′-polarized wave are below its resonance to an y′-polarized incident wave. Moreover, the third resonance to an x′-polarized wave is also less than the second resonance of the cell to y′-polarized wave. However, it is also important that the transmission coefficients of the cell follow the ones depicted in Fig. 4(a), where $S21x'x'$ has two zeros in the middle of the band. The two split rings behave as strongly coupled resonators for x′-polarized incident wave, while they are nonresonant for y′-polarized incident wave for frequencies below 30 GHz. This provides a 180° phase jump only in S21x′x′, between the two working bands, and consequently, enables opposite handedness in the transmitted CP waves in the two bands. The two identical rectangular patches in the same layers are used to achieve the transmission bands for the y′-polarized wave. Finally, the circular slot in the middle layer

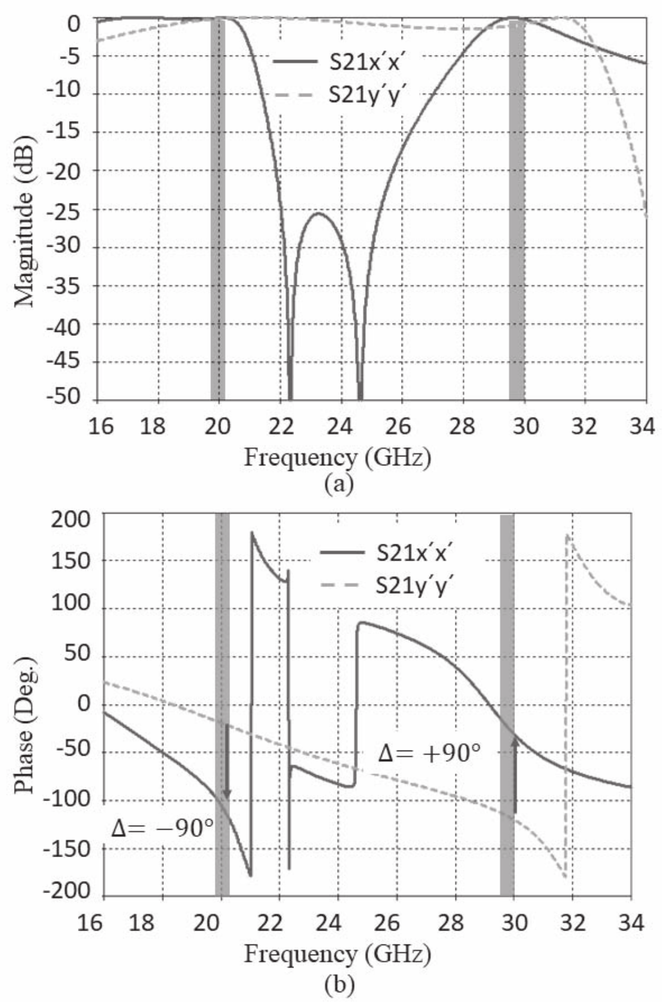

Fig. 4. (a) Amplitude and (b) phase of the transmission coefficients of the UC to an x′-polarized and a y′-polarized normal incident waves.

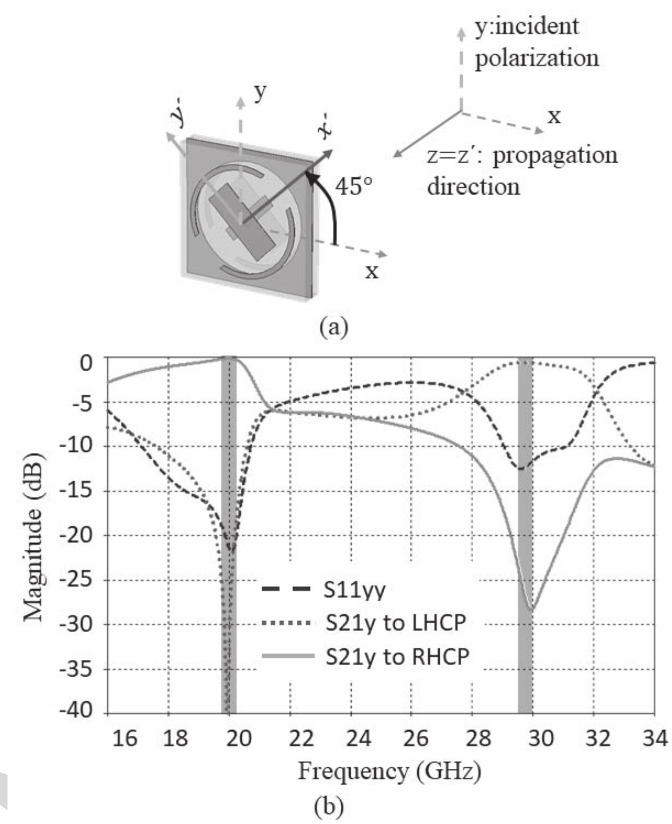

Fig. 5. Reflection coefficient and linear-to-circular transmission coefficients of the UC to y-polarized component normal incident wave and with the cell system of axis rotated by 45° in relation to the incident wave polarization. AQ:5

provides the transmission bands in the lower band. Finally, Fig. 4(b) shows how this arrangement of the resonances allows achieving LP-to-CP conversion with orthogonal handedness at the two bands.

In order to achieve the mentioned resonances, one should choose r_s so that $c/(2\pi r_s\sqrt{\varepsilon_{eff}})$ is lower than the lower frequency band, where c is the speed of light in free space and ε_{eff} is approximated by $(\varepsilon_r + 1)/2$. This ensures that the first resonance in $S11x'x'$ is lower than the desired lower band edge, i.e., 19.7 GHz in the present example. It is worth mentioning that r_s is both the outer radius of the ring and the radius of the slot. This step helps finding the right substrate permittivity ε_r. In the subsequent step, the second resonance in the $S11x'x'$ has to be close to the lower desired frequency band and lower than the first resonance in $S11y'y$. This condition is necessary to obtain −90° phase difference between the two linear transmission coefficients at the lower frequency band (19.7–20.2 GHz). The second resonance in $S11x'x$ is due to the strong coupling between the two split rings and can be achieved and altered by choosing a thinner substrate [30]. Therefore, a substrate thickness based on the available standard commercial size and meeting the previous step can be found. Additional tuning can be done by adjusting the width of the ring, $r_s - r_i$, to shift up this secondary resonance by increasing the width. The third resonance in $S11x'x'$ can be altered by the choice of G_x and G_y so that first, it would be close to the higher desired frequency band, 29.5–30 GHz, and second, it would be lower than the second resonance in $S11y'y'$ (Fig. 3).

For the y′-polarized incident wave, by choosing S, the size of the split in the rings, about $2r_s/3$ and P_y of about $4r_s/3$, the main behavior of the cell to the y′-polarized incident wave is almost defined. One can fine tune S11y′y′ by altering P_x to obtain ±90° phase difference in the transmission coefficient at both frequency bands and ensure that the second resonance of S11y′y′ is slightly higher than the third resonance of the $S11x'x'$. Of course, these guidelines define only the general behavior of the cell and its resonances. After these steps, fine tuning the dimensions through the full-wave simulation of the UC is required to obtain the final results.

B. Linear-to-Circular Polarization Conversion

To assess the insertion loss and the axial ratio of the CP transmitted fields by the polarizer UC, the response of the cell to a y-polarized field [Fig. 5(a)] is presented. The linear reflection and linear-to-circular transmissions of the cell to a y-polarized incident wave are shown in Fig. 5(b).

These coefficients are the same for an x-polarized incident wave but the cell converts the x-polarized of incident wave to an LHCP wave at 20 GHz and to an RHCP wave at 30 GHz with the same coefficients.

Based on Fig. 5(b), the insertion loss of the polarizer cell is 0.1 dB at 20 GHz and 0.6 dB at 30 GHz. This loss is higher at 30 GHz than 20 GHz due to higher reflections of the cell to both LP incident waves (Fig. 3). The bandwidths of the cell, where the reflection coefficient is less than -10 dB and the cross polarization is better than -15 dB, are about 4% (800 MHz) and 8% (2.3 GHz) at 20 and 30 GHz, respectively. The provided bandwidths are much wider than the bandwidths required for *Ka*-band satellite communication highlighted with gray shading in Fig. 5.

It is also important to assess the sensitivity of the cell's performance to the incidence angle. Fig. 6 presents the frequency response of the cell for incident angles up to $\theta_{inc} = 45°$. It is shown that for up to 45° oblique incidence, the transmission loss of the cell increases to only 0.65 dB within 19.7–20.2 GHz [Fig. 6(a)] and 3.2 dB in 29.5–30 GHz [Fig. 6(b)]. Moreover, the dependence of the axial ratio on the incident angle at the lower frequency band and the higher frequency band is presented in Fig. 6(c) and (d), respectively. Fig. 6 shows that the higher increase of transmission loss in the upper band is due to an increase in the reflection coefficient and not by a particular higher depolarization effect of the UC when compared to the lower band. The axial ratio is below 3 and 3.4 dB for incidence angles up to 45° at the lower and higher frequency bands, respectively. However, for incidence angles up to $\theta_{inc} = 30°$, the insertion loss is below 0.2 dB at the lower band and it is below 1.5 dB at the higher band. Moreover, for incidence angles up to $\theta_{inc} = 30°$, the axial ratio is better than 2.3 dB at both bands. While these results are only presented for y-polarized wave, they are also valid for an x-polarized wave but with orthogonal CPs at each band.

IV. Experimental Validation of the Polarizer

An 8×8 array of the LP-to-CP converter UC, introduced in Section III, was fabricated. Each layer was printed on 20 mil Rogers 5880 with 17μm cladding. Then, the printed layers were aligned and glued together with Rogers 3001 bonding film, which has the same relative permittivity as the Rogers 5880 substrate.

To evaluate the performance of the polarizer at both bands, it was first placed in front of a standard gain *K*-band rectangular horn (Flann Microwave N° 20240-15) with 14.4 dBi gain at 20 GHz. Then, it was placed in front of a *Ka*-band standard gain rectangular horn (Flann Microwave N° 22240-15) with the same gain of 14.1 dBi at 30 GHz. Fig. 7 shows the 3-D printed setup to hold the center of the polarizer in front of the center of the horn's aperture and parallel to it. As shown in Fig. 7, the radiation from the horn is y-polarized compared to the polarizer axis. The setup was designed to allow changing the distance between the polarizer and horn to optimize the axial ratio at both bands.

The distance between the polarizer and the horns was first set to $d = 22.5$ mm according to the simulation results.

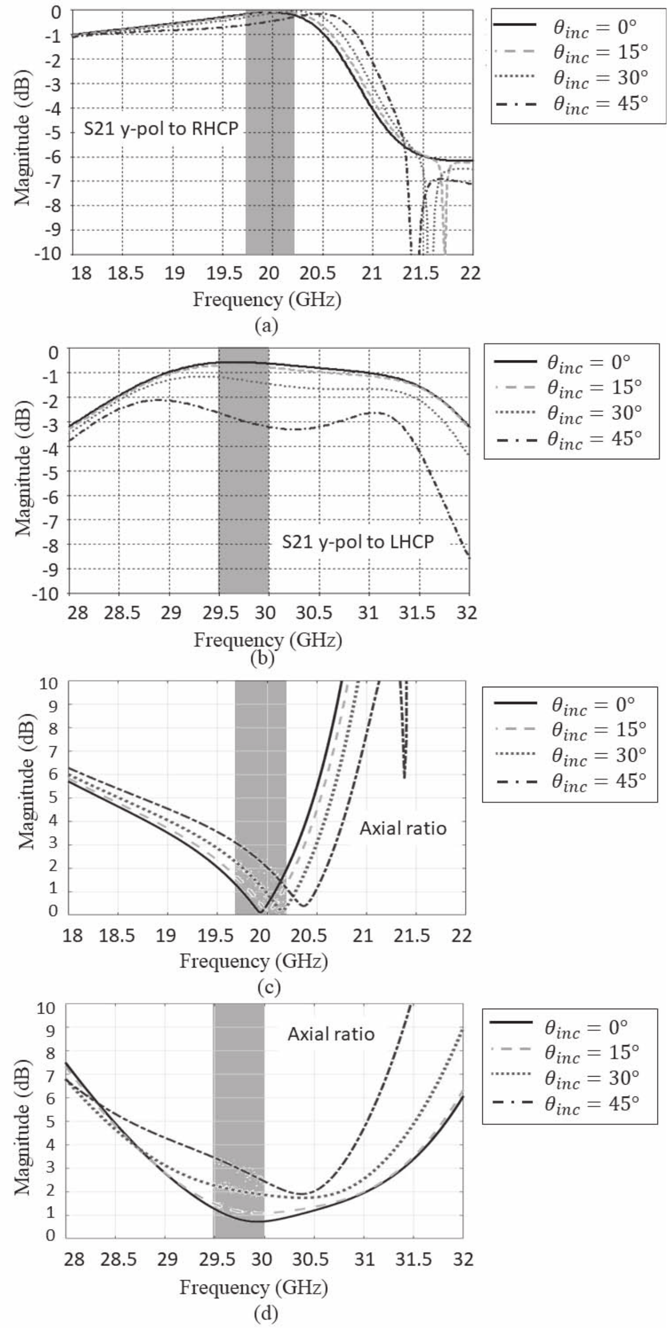

Fig. 6. Performance of the LP-to-CP cell for various incident angles at (a) and (c) lower frequency and (b) and (d) higher frequency bands. (a) y-polarized wave to RHCP transmission coefficient at the lower frequency band. (b) y-polarized wave to LHCP transmission coefficient at the higher frequency band. (c) Axial ratio at the lower frequency band. (d) Axial ratio at the higher frequency band.

However, in the measurements, we also tested $d = 21.3$ mm and $d = 23.7$ mm to find the best axial ratio and gain at both bands. Figs. 8 and 9 present the gain and axial ratio versus frequencies for the above d values, with the polarizer illuminated by the 20 and 30 GHz horns, respectively.

Fig. 8(a) confirms that the y-polarized wave from the horn gets mainly converted through the polarizer to RHCP wave in the lower band. Based on Fig. 8(a) and (b), while the RHCP gain does not change significantly for different

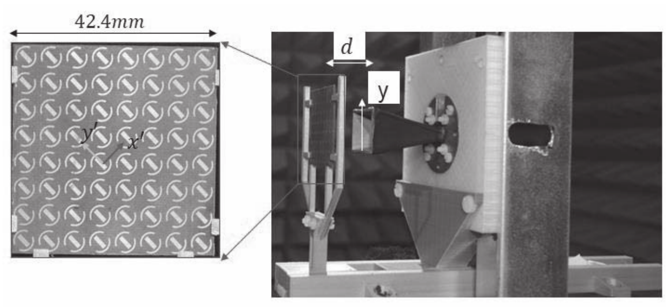

Fig. 7. 3-D printed setup to hold the horn and the polarizer.

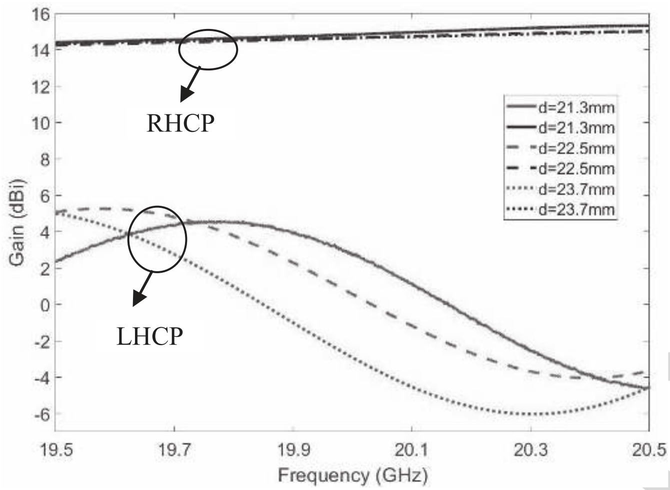

(a)

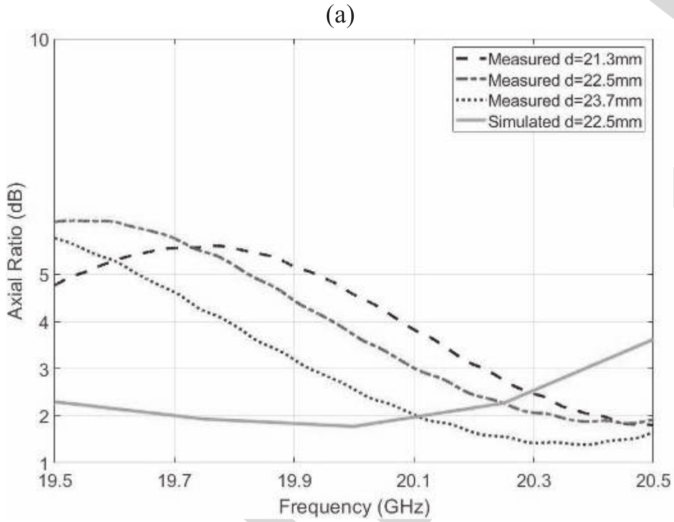

(b)

Fig. 8. (a) Measured CP gains and (b) simulated and measured axial ratio of the 20 GHz horn plus the polarizer at the higher band for different values of *d*.

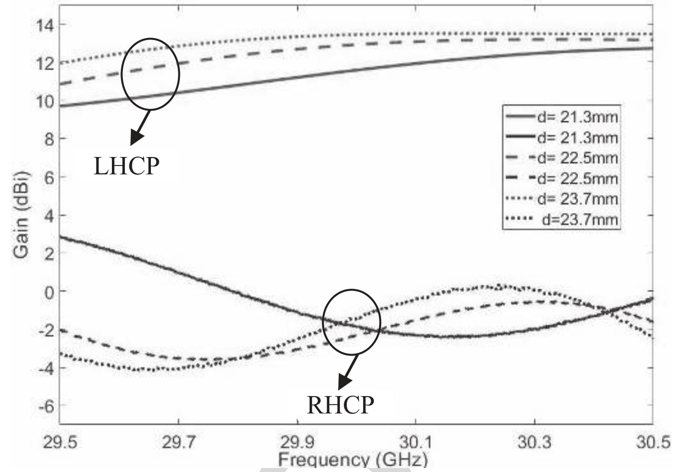

(a)

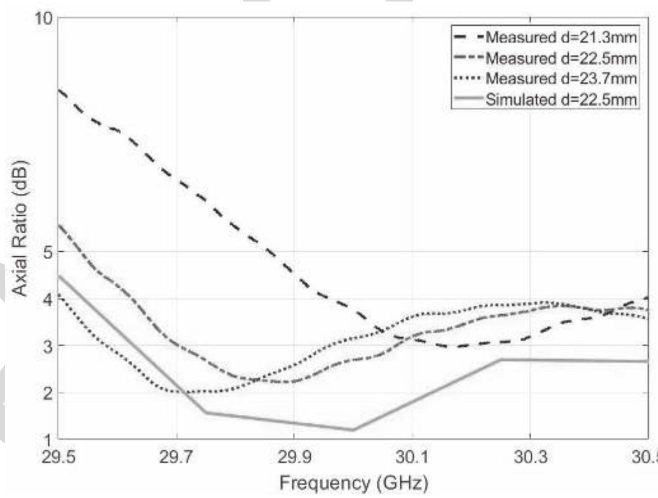

(b)

Fig. 9. (a) Measured CP gains and (b) simulated and measured axial ratio of the 30 GHz horn plus the polarizer at the higher band for different values of *d*.

values of d, the axial ratio is only 1.4 dB at 20.4 GHz for $d = 23.7$ mm. However, the value of d has to be optimized at both bands. Therefore, by looking at Fig. 9(a) and (b), it is obvious that $d = 23.7$ mm also maximizes the gain of LHCP wave at the higher band while it minimizes the gain of the cross RHCP. For this distance, the axial ratio of the 30 GHz horn and the polarizer has the minimum value of 2 dB at 29.7 GHz. Therefore, $d = 23.7$ mm was chosen for the rest of the measurements. It is worth mentioning that Figs. 8(a) and 9(a) confirm that the polarizer converts y-polarized incidence to RHCP at the lower band and LHCP at the higher band. Moreover, the bigger change in the values of the gain at the higher band stems from two reasons. First, the fact that any physical change in d is electrically larger at the higher band, and second, the reflection coefficient of the polarizer is larger at the higher band that causes more coupling between the aperture of the horn and the polarizer. The amount of this coupling changes with the change of d.

The CP radiation patterns of the polarizer in front of the 20 GHz horn when $d = 23.7$ mm are compared with the horn itself at 20 GHz in Fig. 10. Fig. 10 shows that the polarizer converts the y-polarized wave horn with low-insertion loss and cross-polarization level of 16 dB. Fig. 11 shows the comparison of the measured radiation pattern of the LP horn at 30 GHz with the CP patterns of the polarizer feed by the same horn. Fig. 11 shows the LP-to-CP conversion through the

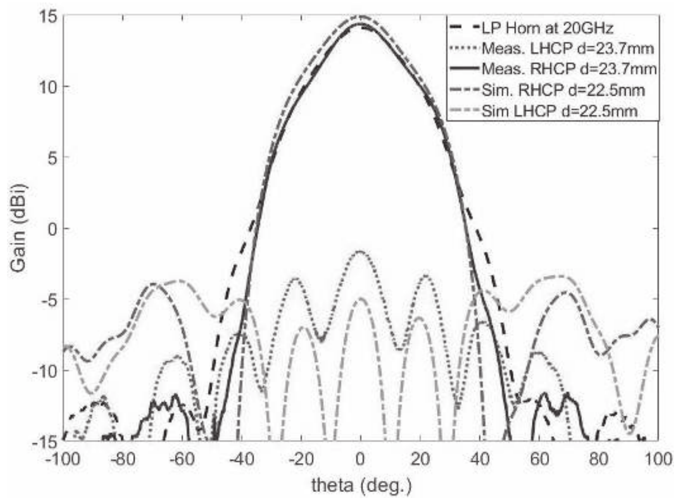

Fig. 10. Measured LP radiation pattern of the 20 GHz horn and simulated and measured CP patterns of the polarizer in front of the horn at, respectively, $d = 22.5$ mm and $d = 23.7$ mm at 20 GHz.

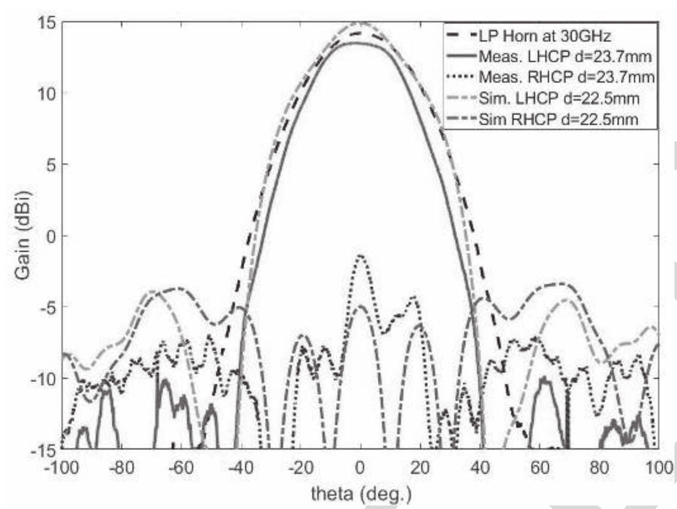

Fig. 11. Measured LP radiation pattern of the 30 GHz horn and simulated and measured CP patterns of the polarizer in front of the horn at, respectively, $d = 22.5$mm and $d = 23.7$mm at 30 GHz.

polarizer at 30 GHz occurs with only 0.7 dB insertion loss and 15 dB of cross-polarization level. Therefore, Figs. 10 and 11 confirm that the polarizer preserves the patterns of each horn and only convert its LP pattern to CP with minimum insertion loss.

V. Integration With a Transmit-Array for Ka-Band Satellite Communications

In this section, we employ the two standard gain LP rectangular horns working at 20 and 30 GHz plus the polarizer as feeds to illuminate a dual-band TA. We will onward call the whole combination of the horn, the polarizer, and the TA, HPTA. The measurements of the HPTA are done at 20.4 and 29.6 GHz based on the measurement results of Section IV and to obtain optimal value of axial ratio from the whole system. The dual-band TA used in this section is similar to the one proposed in [5], where the TA has an aperture size of 196 mm × 147 mm. A 3-D printed support was used to hold the TA at a distance of $F = 100$ mm from the horn and in front of the polarizer. Fig. 12 shows the 3-D setup holding

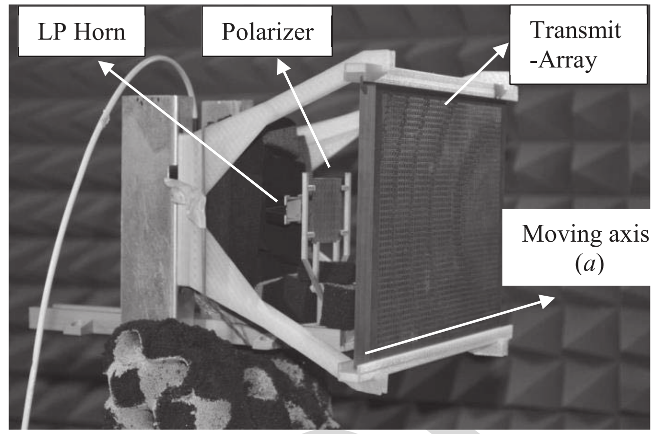

Fig. 12. 3-D printed setup to hold the LP horn, the polarizer, and the dual-band TA. The photograph shows that the setup allows the TA to be moved along the indicated displacement axis to steer the beam.

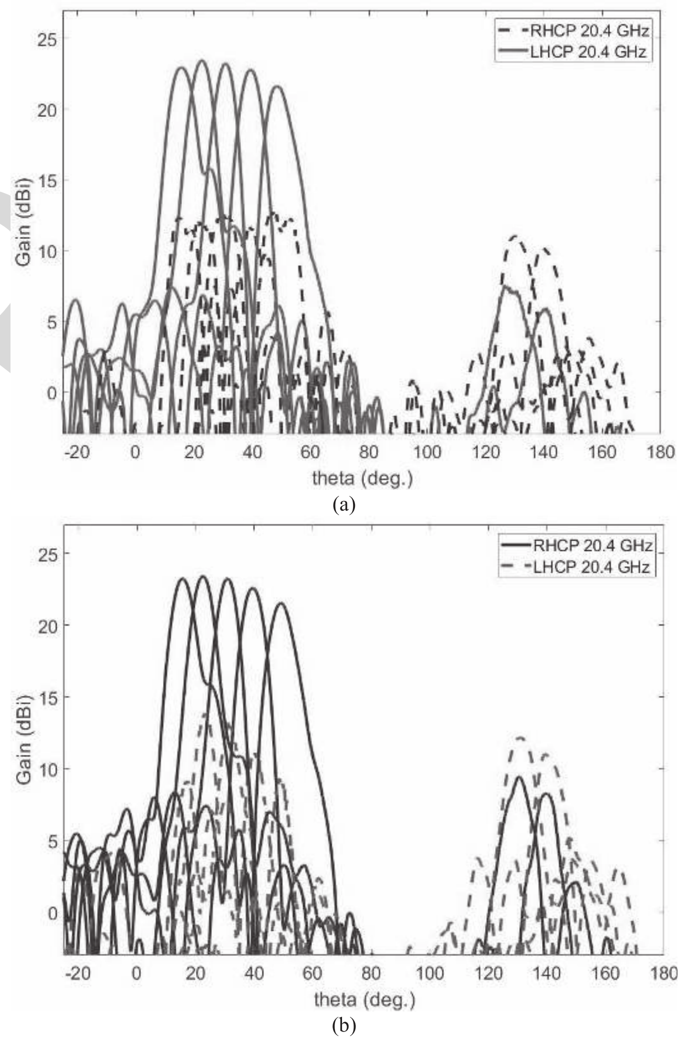

Fig. 13. CP radiation patterns of the 20.4 GHz horn plus the polarizer plus the TA when horn's radiation is (a) x-polarized and (b) y-polarized. Blue lines: RHCP patterns. Red lines: LHCP patterns.

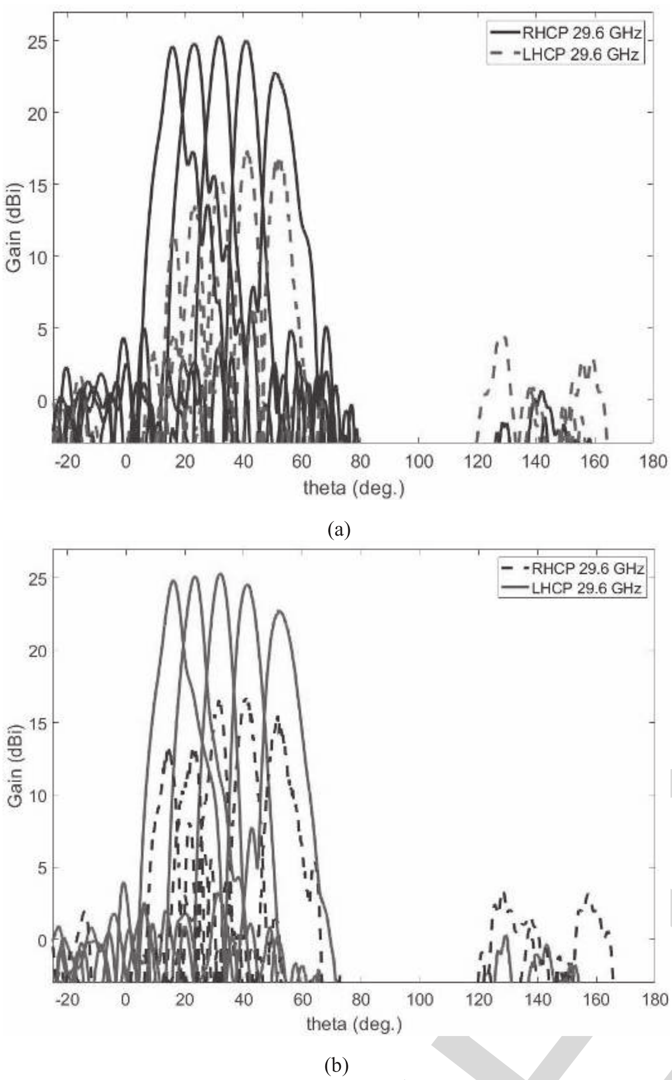

Fig. 14. CP radiation patterns of the 29.7 GHz horn plus the polarizer plus the TA when horn's radiation is (a) x-polarized and (b) y-polarized. Blue lines: RHCP patterns. Red lines: LHCP patterns.

TABLE II

Summary of the Performance of the High-Gain Dual-Band Dual-CP Antenna Composed of the Horn, the Polarizer, and the TA

20 GHz Horn							
LP	***a***	***Polarization***	***Gain (dBi)***	***Beam Direction***	***Scan Loss (dB)***	***X_{pol} (dB)***	***SLL(dB)***
***Polarizer* (Fig. 8)**							
y	0	RHCP	14.4	0º	---	-16	-23.5
***HPTA* (Fig. 13)**							
x	-15	LHCP	21.6	48.56º	-1.8	-8.8	-10.6
	0	LHCP	22.8	39.36º	-0.6	-11.3	-12.6
	15	LHCP	23.2	30.76º	-0.2	-10.7	-17.2
	30	LHCP	23.4	22.56º	0	-11.4	-20.4
	44	LHCP	23.0	15.65º	-0.4	-10.3	-19.2
y	-15	RHCP	21.6	49.06º	-1.8	-12.3	-9.7
	0	RHCP	22.6	39.46º	-0.8	-11.5	-11.6
	15	RHCP	23.2	30.96º	-0.2	-10.3	-16.1
	30	RHCP	23.4	22.56º	0	-9.7	-19.2
	44	RHCP	23.2	15.45º	-0.2	-13.2	-18.3
30 GHz Horn							
LP	***a***	***Polarization***	***Gain (dBi)***	***Beam Direction***	***Scan Loss (dB)***	***X_{pol} (dB)***	***SLL(dB)***
***Polarizer* (Fig. 9)**							
y	0	LHCP	13.5	0º	---	-15	-20.5
***HPTA* (Fig. 14)**							
x	-15	RHCP	22.8	50.96º	-2.5	-6.2	-17.8
	0	RHCP	25.0	40.86º	-0.3	-7.6	-22.6
	15	RHCP	25.3	31.86º	0	-10.1	-19.4
	30	RHCP	24.8	23.26º	-0.5	-11.3	-20.1
	44	RHCP	24.6	15.75º	-0.7	-13.1	-20.5
y	-15	LHCP	22.8	51.96º	-2.6	-8.1	-19.6
	0	LHCP	24.6	41.36º	-0.8	-8.0	-21.6
	15	LHCP	25.4	32.06º	0	-9.3	-23.4
	30	LHCP	25.2	23.36º	-0.2	-12.2	-22.9
	44	LHCP	24.9	16.05º	-0.5	-12.1	-21.2

each horn, the polarizer, and the dual-band TA at the designed distances from each other.

It can be seen from Fig. 12 that the TA can be moved along the shown displacement axis (a) to steer the beam. Here, we moved the TA from $a = -15$ mm to $a = 44$ mm, which corresponds to steering the beam from $\theta = 50°$ to $16°$ at 20 and 30 GHz in the zenith plane. The maximum of the beam is almost directed to the same angle at both frequencies with a difference less than 2°. Fig. 13(a) and (b) shows the CP radiation patterns of the horn, polarizer, and the TA at 20.4 GHz when the horn is x-polarized and y-polarized, respectively. We chose to measure the patterns at 20.4 GHz, since based on Fig. 8(b), the horn plus the polarizer provides minimum axial ratio of 1.4 dB at this frequency. At the end, it can be seen that for both the horn and its 90° rotated one, the HPTA provides maximum gain of 23.4 dBi and scanning loss of less than 1.8 dB in the scanning range of $16° - 50°$. The maximum cross-polarization levels when the horn is x-polarized or y-polarized are 11 and 10 dB, respectively. However, the cross-polarization level is dominated by the behavior of the TA, not only because of the intrinsic behavior of its UCs but also because of the demanding conditions for its operation with reduced F/D and wide-angle scanning. Improving the polarization discrimination of the aperture (TA or other), increasing F/D, and increasing the distance between the LP feed and the polarizer would lead to much lower cross-polarization levels, approaching those of the polarizer under plane-wave excitation. It is worth noticing that orthogonal LP incident waves, here, are obtained by rotating the horn by 90°. However, the same results can be obtained by rotating the polarizer by 90°. Moreover, employing a dual-LP feed eliminates the need for this step.

After measuring the HPTA at the lower band, we replaced the 20 GHz horn with the 30 GHz horn in the 3-D printed support (Fig. 12). Based on both the gain and the axial ratio of the 30 GHz horn with the polarizer (Fig. 9), we performed the measurements at 29.6 GHz, where the gain is 15.8 dBi and the axial ratio is 2.8 dB. Fig. 14(a) shows the CP radiation patterns when the horn is radiating x-polarized wave, and Fig. 14(b) shows the radiation patterns when the horn is 90° rotated. We again moved the TA along a-axis from $a = -15$ mm to $a = 44$ mm to steer the beam at 29.6 GHz. This corresponds to steering the beam from $\theta = 50^\circ$ to 16° with maximum gain of 25.3 dBi and scanning loss of 2.5 dB at 29.6 GHz. The maximum cross-polarization level is 8 dB due to the performance of the TA's elements at this frequency. Finally, Table II summarizes the performance of the HPTA for all the a-positions of the TA with respect to the 20 and 30 GHz horns for both LP radiations.

VI. Conclusion

The possibility of using a single aperture to produce dual-band dual-CP beams, capable of fast toggling of the polarization sense, is very much desired, especially for satellite communications. In this paper, the design complexity of such a primary feed is lowered by using a separate LP feed and a novel passive LP-to-CP polarizer. The proposed polarizer is the focus of this paper. It operates in the transmission mode at two separate nonadjacent frequency bands, converting each orthogonal LP incident waves into orthogonal outgoing CP waves at the two frequency bands. This unique feature of the polarizer allows toggling the polarization sense between the uplink and downlink bands just by switching between two orthogonal incident LP waves. This fulfills completely the above-mentioned requirement in the beginning of the paragraph.

In order to isolate the behavior of the polarizer, in this paper, we used 20 and 30 GHz horns to generate very pure LP incident fields. It was shown that the polarizer reasonably preserves the radiation pattern of the horn while it changes the polarization of the outgoing wave as required. To assess the usefulness of the proposed concept, the horn-plus-polarizer assembly was successfully used to illuminate a K/Ka dual-band TA with CP and wide-angle beam steering.

The separate structure of the primary feed allows great flexibility to use the polarizer in different conditions. For instance, a low-profile printed technology switched dual-LP feed can be used with the same polarizer, instead of the horns. The polarizer can be redesigned for any desired frequency bands and employed separately for various applications. For example, the polarizer itself can be placed in close distance from a dual-band LP reflect array and convert it to dual-band dual-CP reflect array similar to the work done for a single-band RA [32] but for dual-band operation.

Acknowledgment

The authors would like to thank the collaboration from C. Brito and J. Felício for prototype construction. They would like to thank A. Almeida for prototype construction and measurements because without his meticulous work and great patience, implementation of this project was not possible. They would like to thank Rogers Corporation for donating substrates (AQ:7) used for the prototypes. They would also like to thank the Instituto de Plasmas e Fusão Nuclear from Instituto Superior Técnico, University of Lisbon, Lisbon, Portugal, for sharing computational resources.

References

[1] S. Gao, Q. Luo, and F. Zhu, "Introduction to circularly polarized antennas," in *Circularly Polarized Antennas*. London, U.K.: Wiley, 2014, pp. 1–25.

[2] R. Garcia, F. Mayol, J. M. Montero, and A. Culebras, "Circular polarization feed with dual-frequency OMT-based turnstile junction," *IEEE Antennas Propag. Mag.*, vol. 53, no. 1, pp. 226–236, Feb. 2011.

[3] C. A. Leal-Sevillano, J. A. Ruiz-Cruz, J. R. Montejo-Garai, and J. M. Rebollar, "Novel dual-band single circular polarization antenna feeding network for satellite communications," in *Proc. 8th Eur. Conf. Antennas Propag. (EuCAP)*, Apr. 2014, pp. 3265–3269.

[4] E. B. Lima, S. A. Matos, J. R. Costa, C. A. Fernandes, and N. J. G. Fonseca, "Circular polarization wide-angle beam steering at Ka-band by in-plane translation of a plate lens antenna," *IEEE Trans. Antennas Propag.*, vol. 63, no. 12, pp. 5443–5455, Dec. 2015.

[5] S. A. Matos *et al.*, "High gain dual-band beam steering transmitarray for satcom terminals at ka band," *IEEE Trans. Antennas Propag.*, vol. 65, no. 7, pp. 3528–3539, Jul. 2017.

[6] S. Ye *et al.*, "High-gain planar antenna arrays for mobile satellite communications [antenna applications corner]," *IEEE Antennas Propag. Mag.*, vol. 54, no. 6, pp. 256–268, Dec. 2012.

[7] S. Hebib, H. Aubert, O. Pascal, N. J. G. Fonseca, L. Ries, and J. M. E. Lopez, "Multiband pyramidal antenna loaded with a cutoff open-ended waveguide," *IEEE Trans. Antennas Propag.*, vol. 57, no. 1, pp. 266–270, Jan. 2009.

[8] S. D. Targonski, R. B. Waterhouse, and D. M. Pozar, "Design of wide-band aperture-stacked patch microstrip antennas," *IEEE Trans. Antennas Propag.*, vol. 46, no. 9, pp. 1245–1251, Sep. 1998.

[9] Z. Yang and K. F. Warnick, "Multiband dual-polarization high-efficiency array feed for Ku/reverse-band satellite communications," *IEEE Antennas Wireless Propag. Lett.*, vol. 13, pp. 1325–1328, 2014.

[10] A. D. Olver, P. J. B. Clarricoats, and A. A. Kishk, *Microwave Horns and Feeds*. New York, NY, USA: Institution of Electrical Engineers, 1994.

[11] F. F. Manzillo, M. Ettorre, R. Sauleau, and A. Grbic, "Systematic design of a class of wideband circular polarizers using dispersion engineering," in *Proc. 11th Eur. Conf. Antennas Propag. (EUCAP)*, Davos, Switzerland, Mar. 2017, pp. 1279–1281.

[12] S. M. A. M. H. Abadi and N. Behdad, "Wideband linear-to-circular polarization converters based on miniaturized-element frequency selective surfaces," *IEEE Trans. Antennas Propag.*, vol. 64, no. 2, pp. 525–534, Feb. 2016.

[13] L. Martinez-Lopez, J. Rodriguez-Cuevas, J. I. Martinez-Lopez, and A. E. Martynyuk, "A multilayer circular polarizer based on bisected split-ring frequency selective surfaces," *IEEE Antennas Wireless Propag. Lett.*, vol. 13, pp. 153–156, 2014.

[14] M. Euler, V. Fusco, R. Cahill, and R. Dickie, "325 GHz single layer sub-millimeter wave FSS based split slot ring linear to circular polarization convertor," *IEEE Trans. Antennas Propag.*, vol. 58, no. 7, pp. 2457–2459, Jul. 2010.

[15] M.-A. Joyal and J.-J. Laurin, "Analysis and design of thin circular polarizers based on meander lines," *IEEE Trans. Antennas Propag.*, vol. 60, no. 6, pp. 3007–3011, Jun. 2012.

[16] I. Sohail, Y. Ranga, K. P. Esselle, and S. G. Hay, "A linear to circular polarization converter based on Jerusalem-cross frequency selective surface," in *Proc. 7th Eur. Conf. Antennas Propag. (EuCAP)*, Apr. 2013, pp. 2141–2143.

[17] W. Li *et al.*, "A reconfigurable polarization converter using active metasurface and its application in horn antenna," *IEEE Trans. Antennas Propag.*, vol. 64, no. 12, pp. 5281–5290, Dec. 2016.

[18] H. L. Zhu, S. W. Cheung, K. L. Chung, and T. I. Yuk, "Linear-to-circular polarization conversion using metasurface," *IEEE Trans. Antennas Propag.*, vol. 61, no. 9, pp. 4615–4623, Sep. 2013.

[19] M. Mutlu, A. E. Akosman, A. E. Serebryannikov, and E. Ozbay, "Asymmetric chiral metamaterial circular polarizer based on four U-shaped split ring resonators," *Opt. Lett.*, vol. 36, no. 9, pp. 1653–1655, May 2011.

[20] N. J. G. Fonseca and C. Mangenot, "Low-profile polarizing surface with dual-band operation in orthogonal polarizations for broadband satellite applications," in *Proc. 8th Eur. Conf. Antennas Propag. (EuCAP)*, The Hague, The Netherlands, Apr. 2014, pp. 570–574.

[21] N. J. G. Fonseca and C. Mangenot, "High-performance electrically thin dual-band polarizing reflective surface for broadband satellite applications," *IEEE Trans. Antennas Propag.*, vol. 64, no. 2, pp. 640–649, Feb. 2016.

[22] W. Tang, S. Mercader-Pellicer, G. Goussetis, H. Legay, and N. J. G. Fonseca, "Low-profile compact dual-band unit cell for polarizing surfaces operating in orthogonal polarizations," *IEEE Trans. Antennas Propag.*, vol. 65, no. 3, pp. 1472–1477, Mar. 2017.

[23] A. Abbaspour-Tamijani, K. Sarabandi, and G. M. Rebeiz, “Antenna-filter-antenna arrays as a class of bandpass frequency-selective surfaces,” *IEEE Trans. Microw. Theory Techn.*, vol. 52, no. 8, pp. 1781–1789, Aug. 2004.

[24] T. Chaloun, V. Ziegler, and W. Menzel, “Design of a dual-polarized stacked patch antenna for wide-angle scanning reflectarrays,” *IEEE Trans. Antennas Propag.*, vol. 64, no. 8, pp. 3380–3390, Aug. 2016.

[25] P. Naseri, F. Khosravi, and P. Mousavi, “Antenna-filter-antenna-based transmit-array for circular polarization application,” *IEEE Antennas Wireless Propag. Lett.*, vol. 16, pp. 1389–1392, 2017.

[26] P. Naseri, R. Mirzavand, and P. Mousavi, “Dual-band circularly polarized transmit-array unit-cell at X and K bands,” in *Proc. 10th Eur. Conf. Antennas Propag. (EuCAP)*, Davos, Switzerland, Apr. 2016, pp. 1–4.

[27] P. Naseri, C. A. Fernandes, S. A. Matos, and J. R. Costa, “Antenna-filter-antenna-based cell for linear-to-circular polarizer transmit-array,” in *Proc. APS*, San Diego, CA, USA, Jul. 2017, pp. 1071–1072.

[28] P. Naseri, S. A. Matos, J. R. Costa, and C. A. Fernandes, “Phase-delay versus phase-rotation cells for circular polarization transmit arrays—Application to satellite Ka-band beam steering,” *IEEE Trans. Antennas Propag.*, vol. 66, no. 3, pp. 1236–1247, Mar. 2018.

[29] CST Microwave Studio. (Oct. 2014). *Computer Simulation Technology*. [Online]. Available: http://www.cst.com

[30] R. Pous and D. M. Pozar, “A frequency-selective surface using aperture-coupled microstrip patches,” *IEEE Trans. Antennas Propag.*, vol. 39, no. 12, pp. 1763–1769, Dec. 1991.

[31] S. A. Matos, E. B. Lima, J. R. Costa, C. A. Fernandes, and N. Fonseca, “Experimental evaluation of a high gain dual-band beam steerable transmit-array,” in *Proc. 12th Eur. Conf. Antennas Propag. (EuCAP)*, London, U.K., Apr. 2018.

[32] M. Hosseini and S. V. Hum, “A dual-CP reflectarray unit cell for realizing independently controlled beams for space applications,” in *Proc. 11th Eur. Conf. Antennas Propag. (EuCAP)*, Paris, France, Mar. 2017, pp. 66–70.

Parinaz Naseri (M’14) received the B.Sc. degree in electrical engineering (telecommunications) from the University of Tehran, Tehran, Iran, in 2013, and the M.Sc. degree in electromagnetics and microwaves, electrical engineering from the University of Alberta, Edmonton, AB, Canada, in 2017.

From 2016 to 2017, she was a Grant Researcher with the Instituto de Telecomunicações, Lisbon, Portugal. Since 2018, she has been a Researcher with the Reconfigurable Antenna Laboratory, University of Toronto, Toronto, ON, Canada. She has received the Stanley G. Jones Master’s Scholarship in 2014 and the Ontario Trillium Scholarship toward her Ph.D. program at the University of Toronto in 2018. Her current research interests include frequency selective surfaces, transmit arrays, reflectarrays, and polarimetric surfaces.

Sérgio A. Matos (S’05–M’16) received the Licenciado, M.Sc., and Ph.D. degrees in electrical and computer engineering from the Instituto Superior Técnico, University of Lisbon, Lisbon, Portugal, in 2004, 2005, and 2010, respectively.

He is currently a Researcher with the Instituto de Telecomunicações, Lisbon. He is also an Assistant Professor with the Departamento de Ciências e Tecnologias da Informação, Instituto Universitário de Lisboa, Lisbon. He has co-authored 60 technical papers in international journals and conference proceedings. His current research interests include electromagnetic wave propagation in metamaterials, flat-lens design, and transmit arrays.

Jorge R. Costa (S’97–M’03–SM’09) was born in Lisbon, Portugal, in 1974. He received the Licenciado and Ph.D. degrees in electrical and computer engineering from the Instituto Superior Técnico, Technical University of Lisbon, Lisbon, Portugal, in 1997 and 2002, respectively.

He is currently a Researcher with the Instituto de Telecomunicações, Lisbon. He is also an Associate Professor with the Departamento de Ciências e Tecnologias da Informação, Instituto Universitário de Lisboa, Lisbon. He has co-authored four patent applications and more than 150 contributions to peer-reviewed journals and international conference proceedings. More than 30 of these papers have appeared in the IEEE JOURNALS. His current research interests include lenses, reconfigurable antennas, MEMS switches, UWB, MIMO, and RFID antennas.

Dr. Costa served as an Associate Editor for the IEEE TRANSACTIONS ON ANTENNAS AND PROPAGATION from 2010 to 2016. He was a Guest Editor of the Special Issue on *Antennas and Propagation at MM- and Sub MM-Waves* from the IEEE TRANSACTIONS ON ANTENNAS AND PROPAGATION, in 2013. He was the Co-Chair of the Technical Program Committee of the European Conference on Antennas and Propagation (EuCAP 2015) in Lisbon and the General Vice-Chair of EuCAP 2017 in Paris.

Carlos A. Fernandes (S’86–M’89–SM’08) received the Licenciado, M.Sc., and Ph.D. degrees in electrical and computer engineering from the Instituto Superior Técnico (IST), Technical University of Lisbon, Lisbon, Portugal, in 1980, 1985, and 1990, respectively.

In 1980, he joined IST, where he is currently a Full Professor of microwaves, radio wave propagation, and antennas with the Department of Electrical and Computer Engineering. He is currently a Senior Researcher with the Instituto de Telecomunicações, Lisbon, Portugal. He has co-authored over a book, two book chapters, and 180 technical papers in peer-reviewed international journals and conference proceedings. He holds seven patents in the areas of antennas and radiowave propagation modeling. His current research interests include dielectric antennas for millimeter-wave applications, antennas and propagation modeling for personal communication systems, RFID and UWB antennas, artificial dielectrics, and metamaterials.

Dr. Fernandes was a member of the Board of Directors. He was a Guest Editor of the Special Issue on *Antennas and Propagation at MM- and Sub MM-Waves* from the IEEE TRANSACTIONS ON ANTENNAS AND PROPAGATION, in 2013.

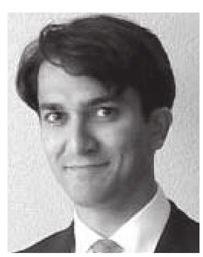

Nelson J. G. Fonseca (M’06–SM’09) was born in Ovar, Portugal, in 1979. He received the M.Eng. degree in electrical engineering from the Ecole Nationale Supérieure d’Electrotechnique, Electronique, Informatique, Hydraulique et Telecommunications, Toulouse, France, in 2003, the M.Sc. degree in electrical engineering from the Ecole Polytechnique de Montréal, Montreal, QC, Canada, in 2003, and the Ph.D. degree in electrical engineering from the Institut National Polytechnique de Toulouse, Université de Toulouse, Toulouse, in 2010.

He was an Antenna Engineer with the Department of Antenna Studies, Alcatel Alénia Space, Toulouse (now Thalès Alénia Space). He was with the Antennas Section, French Space Agency, Toulouse. In 2009, he joined the Antenna and Sub-Millimeter Wave Section, European Space Agency, Noordwijk, The Netherlands. He has authored or co-authored over 150 papers in journals, conferences, and specialized workshops. He contributed to 18 technical innovations, protected by over 30 patents issued or pending. His current research interests include multiple beam antennas for space missions, beam-formers theory and design, and new enabling technologies such as metamaterials.

Dr. Fonseca was a recipient of several prizes, including the Best Young Engineer Paper Award at the 29th ESA Workshop on Antennas in 2007. He is currently serving as a Technical Reviewer for several journals, including the IEEE TRANSACTIONS ON ANTENNAS AND PROPAGATION and the IEEE TRANSACTIONS ON MICROWAVE THEORY AND TECHNIQUES.

AUTHOR QUERIES

PLEASE NOTE: We cannot accept new source files as corrections for your paper. If possible, please annotate the PDF proof we have sent you with your corrections and upload it via the Author Gateway. Alternatively, you may send us your corrections in list format. You may also upload revised graphics via the Author Gateway.

AQ:1 = Author: Please confirm or add details for any funding or financial support for the research of this article.
AQ:2 = Please note that current affiliation for "Parinaz Naseri" does not match from the F.F. to the bio. Please check and confirm.
AQ:3 = Please confirm whether the authors affiliation details are correct as set.
AQ:4 = Please confirm whether the edits made in this part "therefore, it is a very good..." retains the intended meaning.
AQ:5 = Please provide the subpart description for Fig. 5.
AQ:6 = Please provide an expansion for "HPTA."
AQ:7 = Please provide location for "Rogers Corporation."
AQ:8 = Please provide the page range for ref. [31].